

Filtering amplitude dependence of correlation dynamics in complex systems: application to the cryptocurrency market

Marcin Wątorek*

*Faculty of Computer Science and Mathematics, Cracow University of Technology, Kraków, Poland and
Adapt Research Centre, School of Computing, Dublin City University, Dublin, Ireland*

Marija Bezbradica and Martin Crane

Adapt Research Centre, School of Computing, Dublin City University, Dublin, Ireland

Jarosław Kwapienie

Complex Systems Theory Department, Institute of Nuclear Physics, Polish Academy of Sciences, Kraków, Poland

Stanisław Drożdż†

*Complex Systems Theory Department, Institute of Nuclear Physics,
Polish Academy of Sciences, Kraków, Poland and*

Faculty of Computer Science and Mathematics, Cracow University of Technology, Kraków, Poland

(Dated: October 29, 2025)

Based on the cryptocurrency market dynamics, this study presents a general methodology for analyzing evolving correlation structures in complex systems using the q -dependent detrended cross-correlation coefficient $\rho(q, s)$. By extending traditional metrics, this approach captures correlations at varying fluctuation amplitudes and time scales. The method employs q -dependent minimum spanning trees (q MSTs) to visualize evolving network structures. Using minute-by-minute exchange rate data for 140 cryptocurrencies on Binance (Jan 2021–Oct 2024), a rolling window analysis reveals significant shifts in q MSTs, notably around April 2022 during the Terra/Luna crash. Initially centralized around Bitcoin (BTC), the network later decentralized, with Ethereum (ETH) and others gaining prominence. Spectral analysis confirms BTC's declining dominance and increased diversification among assets. A key finding is that medium-scale fluctuations exhibit stronger correlations than large-scale ones, with q MSTs based on the latter being more decentralized. Properly exploiting such facts may offer the possibility of a more flexible optimal portfolio construction. Distance metrics highlight that major disruptions amplify correlation differences, leading to fully decentralized structures during crashes. These results demonstrate q MSTs' effectiveness in uncovering fluctuation-dependent correlations, with potential applications beyond finance, including biology, social and other complex systems.

I. INTRODUCTION

The fundamental characteristic of complex systems is the nonlinear interactions between their constituent elements [1, 2]. In such systems, the evolution is typically driven by the presence of multiple generators. As a result, the signals recorded from such systems typically comprise a convolution of effects induced by different generators, where different ones may dominate at different times. This complexity emerges frequently in the form of multifractality, particularly when some of the generators exhibit a hierarchical structure such as in a multiplicative cascade [3]. In such cases, complexity may be encoded in the nonlinear temporal dependencies within the sequence of signal fluctuations, but also in their amplitude, which can strongly be influenced by the temporal dependencies. It is often more pronounced in fluctuations within a certain amplitude range rather than in those outside of it. Typically, fluctuations of relatively large size exhibit a more complex structure compared to small-size fluctuations, which are often overwhelmed by background noise [4]. From the perspective of identifying complexity in the recordings of a given observable, it is crucial to employ a tool capable of distinguishing data that are relevant to the structural complexity from those that are not. In this regard, signal filtering procedures can be utilized to extract the signatures of complexity, facilitating a more accurate characterization of the underlying dynamical processes. In this work, we apply one such tool based on the multiscale detrended cross-correlation coefficient and graph theory to a structural study of the cryptocurrency market [5, 6].

* Contact author: marcin.watorek@pk.edu.pl

† Contact author: stanislaw.drozd@ifj.edu.pl

More than a decade after the introduction of the first cryptocurrency using blockchain technology, Bitcoin, the market for these assets exhibits many characteristics of a mature market. Such characteristics include liquidity [7–9], power-law tails in probability density distributions [10–12] and multiscaling [8, 13–17]. In addition to these, similarities with other financial markets has been noted e.g. a level of efficiency [18–20] and also significant correlation with such markets [10, 21–27]. This last characteristic prevents cryptocurrencies from being considered a safe haven for hedging investments [21, 26, 28, 29].

Like any financial market where multiple assets are traded, the cryptocurrency market exhibits an internal structure [8]. From an investor’s perspective individual cryptocurrencies vary in significance with respect to factors such as trust, the governing consensus algorithm of the blockchain, transaction liquidity, and market capitalization. Moreover, investors in the cryptocurrency market tend to behave irrationally and are easily influenced by price changes, as well as concrete news items. This contrasts with traditional markets (e.g. stocks, commodities and currencies) where the dominance of professional investors exists. This results in more frequent herding behaviour among cryptocurrency price changes [30]. Beyond this, groups of cryptocurrencies can be distinguished with different levels of internal coupling [31–37]. If this coupling is measured using correlation metrics between observables representing cryptocurrencies, such as returns, volatility, or transaction volume, it is possible to identify sectors within the market composed of cryptocurrencies with either similar characteristics or those treated similarly by investors. By using these correlation measures to represent the market as a network, a hierarchical structure emerges, where some cryptocurrencies play a central role in the network while others are secondary, tertiary, or peripheral. The most significant hubs that have been consistently identified across different studies are the most capitalized cryptocurrencies: BTC and ETH. The market sectors become network clusters and they are typically related to some secondary assets that play the role of the sectorial hubs [38–41]. This structure is not stable but rather dynamic and evolves over time, however [42–47].

Cross-correlation networks representing financial markets typically consist of a large number N of nodes, each corresponding to a single asset, and an even greater number of weighted edges representing connections between individual asset pairs. In such cases, analyzing and especially visualizing the entire network quickly becomes cumbersome and unreadable. To address this issue, filters are applied to the complete network, removing insignificant or less relevant edges while retaining those that are crucial to the structure. There are many different types of such filters, varying in the number of nodes and edges they preserve and, thus, in the amount of information they retain. Among these, one can list a minimal spanning tree (MST) [48–50], a planar maximally filtered graph (PMFG) [51–53], a triangulated maximally filtered graph (TMFG) [40, 54, 55], and a correlation-threshold graph [56–58]. Moreover, in addition to traditional correlation-based methods, more sophisticated measures based on distances between structural breaks [59] and change points [60] may also be considered as a base to network construction. However, it should be remembered that in order to be used here, these measures must satisfy the known three mathematical conditions of a metric, which may not always be possible. The measure based on the ρ_q coefficient satisfies these conditions [61, 62].

Due to its structure and the small number of edges, the most commonly used filter is the minimum spanning tree (MST) [48]. It is a subnetwork of the complete network, consisting of N nodes and $E = N - 1$ edges, where the sum of the weights of all its edges is minimized. MST is constructed using either Prim’s algorithm [63] or Kruskal’s algorithm [64]. The former performs better in dense networks ($E \sim N^2$) due to its $O(E + N \log N)$ complexity, while the latter is more efficient for sparse networks ($E \sim N$), with a complexity of $O(E \log N)$. The filter based on MST has been successfully used to analyze correlation structure in financial markets, such as stock markets [49, 65–72], the foreign exchange market [50, 73–78], commodity markets [79–82], as well as the cryptocurrency [38, 39, 42, 83–86] and NFT markets [87, 88]. As regards the cryptocurrency market, listed in what follows are a few examples of such MST-based studies.

By examining the relationships among 100 cryptocurrencies in the years 2018–2019, expressed through cross-correlation coefficients and a measure of dissimilarity between periodograms for returns and volatility, it was demonstrated that the cryptocurrency market, represented by MST trees, has a hierarchical structure with a high degree of centralization, where the largest-capitalization coins were found to act as hubs [83]. A similarly sized group of 119 cryptocurrencies represented by daily data from the years 2016–2018 also exhibited a hierarchical structure but with significantly lower centralization [38]. Based on a small set of 16 cryptocurrencies and the Pearson cross-correlation coefficients, a centralized market structure was reported for daily data from 2017–2018, with ETH as the dominant node [84]. This transient dominant position of ETH as the network center was not an isolated event, as the situation repeated itself at the beginning of 2019 [43] and at the turn of 2020–2021 [44]. A study of cross-correlations within a set of 78 cryptocurrencies from 2015–2018 showed a developed sectoral structure already at that time. Furthermore, it was observed that BTC was relatively insensitive to external shocks and had little impact on the evolution of other cryptocurrencies. More influential assets were dogecoin (DOGE) and litecoin (LTC) [39].

Based on daily data from the years 2017–2018, a core-periphery structure in a network of 157 cryptocurrencies was identified, where the most capitalized coins were shifted to the periphery, while some less capitalized ones formed the center; this structure was explained through the trading properties of each coin [85]. In an analysis of high-frequency

data for 76 cryptocurrencies collected over several months at the turn of 2017-2018, a clear dominance of BTC and ETH hubs was observed, which masked more subtle relationships among the remaining cryptocurrencies. In order to counter this effect, MST trees based on residual data after filtering out the influence of these two dominant assets were subsequently constructed. The residual structure had a strongly sectoral form with six distinguishable sectors, some of which were relatively stable and invariant to regulatory changes affecting the market during the studied period, while others had a more ephemeral nature [42]. In another study, daily data for 136 cryptocurrencies was examined by using various correlation measures and constructing the related MSTs. The results demonstrated differences in the evolution of market structure depending on the correlation measure used. An increasing market correlation with rising market capitalization for some measures was reported, while other measures exhibited significantly greater randomness [86]. Daily price variations of a large set of 1000 cryptocurrencies with the largest capitalization were analyzed in order to investigate the reliability of constructing optimal portfolios based on cross-correlations among these cryptoassets. However, it was impossible to develop a profitable long-term investment by using this approach, because of a high degree of instability of the market cross-correlation structure, which required rebuilding the portfolios daily [46]. As the final example, a growing centralization of tokens (cryptocurrencies, DeFi's, and NFTs) on the Ethereum platform in agreement with the rich-get-richer paradigm was found in yet another recent study using the MST filtering [87].

The standard MST approach, which applies the Pearson cross-correlation coefficient as a measure of bivariate interdependence between time series, proves problematic for nonstationary data as the results can be unreliable [62]. Trends represent a prominent source of statistical nonstationarity if present in the time series. Thus, they need to be eliminated first. The most popular framework to deal with trends is detrended fluctuation analysis (DFA) [89] together with its multiscale generalization - multifractal detrended fluctuation analysis [90]. Together with its bivariate variant - multifractal detrended cross-correlation analysis (MFCCA) [91-93] - these two latter methods can be combined in order to define a q -dependent detrended cross-correlation coefficient ρ_q , which may be used as a direct counterpart of the Pearson coefficient for nonstationary data ρ_{DCCA} if $q = 2$. However, since $q \in \mathbb{R}$, the new measure offers much more than that. By adjusting the value of the parameter q , one can select the magnitude of local variances of the detrended signals and focus only on their selected parts. In this way, the cross-correlation structure of the analyzed data may be broken down to a specific range of amplitudes only [61]. With the use of ρ_q , one may proceed to multivariate sets, construct the corresponding q -dependent cross-correlation matrix, and finally, arrive at the definition of the q -dependent detrended MST constructed in the same way as the regular MSTs but here based on the q -order detrended cross-correlations [62, 94].

The q -dependent detrended minimum spanning trees (q MSTs) were proposed as a tool for visualizing a selective cross-correlation structure of multivariate non-stationary time series filtered based on fluctuation magnitude [62]. It was shown that, by applying the q -dependent detrended cross-correlation coefficient ρ_q to time series representing stock returns of the largest US companies, it was possible to extract genuine information on the cross-correlation structure of the US market that could not be obtained based on the detrended cross-correlation coefficient ρ_{DCCA} . It was also shown that the q MST topology could differ substantially between the graphs constructed for different values of q . For small and medium returns ($q \leq 2$), the respective q MSTs had a centralized structure, while large returns ($q > 2$) developed trees the more dispersed, the larger return amplitude was considered [62].

There are a few studies available in literature, in which the idea of q MSTs have been successfully exploited. Zhao et al. [95] analyzed the cross-correlation structure of price returns for a set of 401 S&P500-constituent stocks and Lin et al. [96] studied cross-correlations between 37 world stock-market indices representing major economies by focusing on fluctuations of different magnitude. In these works, planar maximally filtered graphs (PMFGs [51]) based on the q -dependent detrended cross-correlation coefficient ρ_q were constructed. Like their standard counterparts do with MSTs, these q PMFGs contain q MSTs as their subnetworks created in the initial step of the construction algorithm. Quite surprisingly, in both the S&P500 stocks and the world indices, the obtained results showed that small returns are cross-correlated more strongly than the large ones, a result that has seldom been reported in literature. However, different subsets of stocks and different subsets of indices were correlated in each case. From the node degree perspective, the returns of small or medium amplitude formed networks with significant heterogeneity, while large returns revealed networks that were much more homogeneous. Application of the obtained q PMFGs to optimal portfolio selection under the mean-variance framework by using centrality measures as the selection metric showed that portfolios based on peripheral stocks outperform the ones based on central stocks with $q = 2$ as the best choice under the condition of the largest difference in network topology. However, the same analysis carried out under the expected shortfall framework pointed out to the values $2 \leq q \leq 6$ instead [95].

q MST trees themselves were then applied to study the structure of cross-correlations in the cryptocurrency market [44]. High-frequency data for the 80 largest-capitalization cryptocurrencies traded on the Binance exchange were analyzed using a rolling window to determine changes in the correlation structure over time during the years 2020-2021. This structure underwent significant changes during that period, becoming increasingly centralized. For short time scales on the order of minutes, the q MST tree structure was found to have a single star-like shape centered on either BTC or ETH. These shifts between the two main cryptocurrencies were rare for these time scales, and the networks

remained relatively stable. However, the situation was entirely different for longer time scales, on the order of several hours, where the central hub frequently changed, switching among the most liquid cryptocurrencies. In addition to BTC and ETH, assets such as ontology (ONT), tron (TRX), and FTX token (FTX) also played central roles. The results also showed that while the cryptocurrency market was relatively independent of other financial markets at the onset of the pandemic, as markets ed to the pandemic and its impact decreased, inter-market cross-correlations became strong again.

In this work, a set of time series representing price returns of highly capitalized cryptocurrencies is analyzed by means of the coefficient ρ_q and the q MST graphs in order to investigate the temporal evolution of the cross-correlation structure of the cryptocurrency market. The paper is organized as follows: in Sect. II, the essential information regarding the MFDFA/MFDCCA methodology, the coefficient ρ_q , and the q MST graph is provided together with a brief description of the datasets used. In Sect. III the results are reported and discussed, while conclusions and future research perspectives are presented in Sect. IV.

II. DATA AND METHODS

A. Multifractal detrended cross-correlation analysis

It happens frequently that empirical time series recorded from observables related to natural complex systems reveal a multifractal organization of fluctuations [4, 69]. Identification and quantification of such an organization in time series requires a properly designed methodology that is able to grasp the genuine effects and neglect spurious ones. It has already been demonstrated that one of the possible choices in this respect is MFDFA/MFDCCA, a methodology that proved to be effective and reliable [90, 92, 93, 97, 98]. It is based on observing scaling properties of the moments of time series that have been detrended. This methodology can be described as follows. Let one consider two time series $U = \{u(i)\}_{i=1}^T$ and $V = \{v(i)\}_{i=1}^T$ of length $T \gg 1$ that are sampled at the same time instants i . First, both time series are integrated to form their profiles \tilde{U} and \tilde{V}

$$\tilde{u}(i) = \sum_{j=1}^i u(j), \quad \tilde{v}(i) = \sum_{j=1}^i v(j), \quad (1)$$

respectively. These time series can be divided into M_s segments of length s each starting from both their beginnings and their ends in order not to neglect any data points, so there are $2M_s$ segments total. Next, a detrending procedure is applied, in which a polynomial trend $P_\nu^{(m)}$ of order m is subtracted from \tilde{U} and \tilde{V} in each segment ν independently:

$$\begin{aligned} x(\nu s + k) &= \tilde{u}(\nu s + k) - P_{X,\nu}^{(m)}(k), \\ y(\nu s + k) &= \tilde{v}(\nu s + k) - P_{Y,\nu}^{(m)}(k), \end{aligned} \quad (2)$$

where $k = 1, \dots, s$ and $\nu = 0, \dots, 2M_s - 1$. In the subsequent step, segment-wise covariance f_{XY}^2 and variances f_{XX}^2 , f_{YY}^2 are calculated

$$\begin{aligned} f_{XY}^2(s, \nu) &= \frac{1}{s} \sum_{k=1}^s x(\nu s + k) y(\nu s + k), \\ f_{XX}^2(s, \nu) &= \frac{1}{s} \sum_{k=1}^s x^2(\nu s + k), \\ f_{YY}^2(s, \nu) &= \frac{1}{s} \sum_{k=1}^s y^2(\nu s + k). \end{aligned} \quad (3)$$

Then a family of bivariate fluctuation functions F_{XY}^q and univariate ones F_{XX}^q , F_{YY}^q is obtained by raising, respectively, f_{XY}^2 , f_{XX}^2 , and f_{YY}^2 to a real power q and taking averages over the segments:

$$\begin{aligned} F_{XY}^q(s) &= \left\{ \frac{1}{2M_s} \sum_{\nu=0}^{2M_s-1} \text{sign}[f_{XY}^2(s, \nu)] |f_{XY}^2(s, \nu)|^{q/2} \right\}^{1/q}, \\ F_{XX}^q(s) &= \left\{ \frac{1}{2M_s} \sum_{\nu=0}^{2M_s-1} [f_{XX}^2(s, \nu)]^{q/2} \right\}^{1/q}, \\ F_{YY}^q(s) &= \left\{ \frac{1}{2M_s} \sum_{\nu=0}^{2M_s-1} [f_{YY}^2(s, \nu)]^{q/2} \right\}^{1/q}. \end{aligned} \quad (4)$$

The sign function in the first formula in Eq. (4) has been introduced in order to guarantee that the fluctuation functions remain real for any choice of the parameter q , but also for consistency of the results [93].

All the steps described so far are repeated for different values of the segment length s . If the time series X, Y are fractal, the univariate fluctuation functions F_{XX}^q , F_{YY}^q show a power-law dependence on s [90]:

$$F_{XX}^q(s) \sim s^{h_X(q)}, \quad F_{YY}^q(s) \sim s^{h_Y(q)}. \quad (5)$$

The exponents $h_X(q)$ and $h_Y(q)$ are non-increasing functions of q and are called the generalized Hurst exponents, because they coincide with the Hurst exponent H for $q = 2$. Based on their behaviour, the following two cases can be distinguished: a monofractal scaling if $h_X(q) = \text{const}$ and a multifractal one if $h_X(q)$ is monotonously decreasing in q . If, in addition, the bivariate fluctuation function F_{XY}^q defined by the following formula

$$F_{XY}^q(s) \sim s^{\lambda_{XY}(q)}, \quad (6)$$

shows scaling, the two time series X, Y are said to be monofractally cross-correlated if $\lambda_{XY}(q) = \text{const}$ or multifractally cross-correlated otherwise. The parameter $q \in \mathbb{R}$ plays an important role in allowing for the extraction of fluctuations within the amplitude range of interest by selectively amplifying them and attenuating those in other amplitude ranges. The standard case corresponding to equally weighted fluctuations is obtained for $q = 2$.

B. q -dependent detrended minimum spanning trees

The univariate and bivariate fluctuation functions can be used to define the q th-order detrended cross-correlation coefficient $\rho_q(s)$

$$\rho_q(s) = \frac{F_{XY}^q(s)}{\sqrt{F_{XX}^q(s)F_{YY}^q(s)}}. \quad (7)$$

introduced in [61] as a generalization of the detrended cross-correlation coefficient ρ_{DCCA} [99]. The role of the parameter q is similar to the one it plays in the case of the fluctuation functions. However, while in principle $q \in \mathbb{R}$ also in this case, there are some subtleties regarding the behaviour of the coefficient for different ranges of q . For $q \geq 0$, values of $\rho_q(s)$ satisfy the condition $-1 \leq \rho_q \leq 1$, which is not the case for $q < 0$, where the coefficient may assume values outside this range (for more information, see [61]). However, consideration of such a situation is beyond the scope of the present study, in which we restrict our analysis to $q \geq 0$. It is important to note that, being a function of scale, the coefficient $\rho_q(s)$ does not require the fluctuation functions used in its calculation to exhibit a power-law dependence, which makes it a robust tool that can also be used for non-fractal time series. The formula (7) implies invariance of $\rho_q(s)$ under a swap of time series $X \leftrightarrow Y$.

In a multivariate case, when N parallel time series are of interest, in order to obtain a complete correlation map, one has to compute $N(N - 1)/2$ values of $\rho_q(s)$ for each considered time scale s . It is thus convenient to arrange these values in an $N \times N$ matrix $\mathbf{C}(q, s)$ with elements $C_{ij}(q, s) \equiv \rho_q^{ij}(s)$, which may be considered as a q -dependent detrended cross-correlation matrix ($i, j = 1, \dots, N$). It can be diagonalized and its eigenvalues λ_i and eigenvectors \mathbf{v}_i can be obtained by using the formula

$$\mathbf{C}(q, s)\mathbf{v}_i(q, s) = \lambda_i(q, s)\mathbf{v}_i(q, s). \quad (8)$$

Due to the fact that $\rho_q(s)$ cannot be used as a metric (similar to the Pearson correlation coefficient, ρ_q doesn't satisfy the triangle inequality condition for time series triples), one has to redefine the matrix elements $C_{ij}(q, s)$ to

partially address this issue:

$$D_{ij}(q, s) = \sqrt{2[1 - C_{ij}(q, s)]}, \quad (9)$$

where $D_{ij}(q, s)$ are the elements of a distance matrix $\mathbf{D}(q, s)$. Now these elements satisfy the triangle inequality if $q \geq 1$ (see [62] for a related discussion).

Based on the matrix $\mathbf{D}(q, s)$, one may construct a weighted, undirected network \mathcal{N} consisting of N nodes, with each node representing a time series under study. Then, by applying Kruskal's or Prim's algorithm [48, 63, 64] to the elements $D_{ij}(q, s)$ for fixed q and s , one can extract a subset of \mathcal{N} with the same number of nodes and $N - 1$ undirected edges that minimize the edge weight sum. This subset is called the q -dependent detrended minimum spanning tree (q MST) of \mathcal{N} [62, 94]. As being based on the coefficients $\rho_q(s)$, q MST is sensitive, by construction, to the segment-wise detrended covariances (Eq. (3)) of the considered multivariate time series. Therefore, one can focus on a particular range of covariances by amplifying the relative contribution of particular segments ν to $F_{XY}^q(s)$ and suppressing the relative contribution of the remaining ones. In consequence, a resulting q MST may reflect the multivariate structure of, for example, strong ($q > 2$) or moderate ($q < 2$) covariances rather than the overall average covariance structure ($q = 2$). Although small covariances ($q < 0$) cannot be selected in this way due to the necessary condition $q \geq 1$ for q MST, this does not pose a problem because small covariances are likely statistically insignificant. In the empirical part of the paper, two representative values $q = 1$ and $q = 4$ will be considered. In the case of $q = 1$, there is no additional relative amplification of fluctuations [61], thus the average fluctuations play the most significant role. The value of $q = 4$ was chosen in order to amplify the effect of large fluctuations relative to the smaller ones. In the present case this value of q also sets the upper limit allowing the convergence of moments [100]. For $q > 4$, the moments may diverge due to the inverse cubic power-law (tail exponent of about 3) governing the asymptotic distribution of large returns [101], also in the cryptocurrency exchange rates case [12].

C. Data specification

The data set comprises $N = 140$ exchange rates of the most traded cryptocurrencies expressed in USDT on the Binance exchange [102], covering the period from January 1, 2021 to September 30, 2024 (the data are available in an open repository [103]). As Binance is the largest exchange with the highest volume value [104], the data set includes all highly capitalized cryptocurrencies and thus it is representative of the entire cryptocurrency market. The stablecoins were excluded from the analysis because their volatility relative to USDT is minimal.

The time series were sampled at 1-minute frequency. The exchange rate time series were first transformed into logarithmic returns $R_i(t_m) = \ln p_i(t_{m+1}) - \ln p_i(t_m)$, where $m = 1, \dots, T - 1$ and i represents a specific cryptocurrency ticker. The complete list of the cryptocurrency tickers considered in this study, along with their respective sectors according to the CoinDesk classification [105], is provided in Appendix A in Tab. I. Basic statistics for each of the exchange rate are also included: the average volume value $\langle V_{\Delta t} \rangle$, the average number of transactions $\langle N_{\Delta t} \rangle$, and the fraction of zero log-returns $\%0R_{\Delta t}$ for $\Delta t = 1\text{min}$. There are visible significant differences between cryptocurrencies in average volume and trading frequency in the data set considered. BTC has the first position in both statistics, and ETH is clearly 2nd, with a significant gap to the rest.

The evolution of the cumulative logarithmic returns $\hat{R}(t_m) = \sum_{m=1}^T R(t_m)$ of the 140 cryptocurrencies over the analyzed time period is presented in Fig. 1. Various phases of the market can be observed. The bull market in 2021, then the bear market in 2022, with the crash in May 2022. After reaching its bottom at the end of 2022, the market was in a slower growth phase until mid-2024, then moved sideways until the end of September 2024. Thus, the selected dataset allows for market analysis under various conditions.

III. RESULTS

A. Changes in cross-correlations over time

To track the evolution of cross-correlations, a rolling window of 7 days - trading week (10,080 data points) was applied, with a daily step (1,440 data points) along the time series. In each rolling window, $\mathbf{C}(q, s)$ (Eq. 8) was calculated and then transformed into $\mathbf{D}(q, s)$ (Eq. 9), from which the q MST graph was constructed. Then, the spectral and network characteristics were calculated for them. These include the largest eigenvalue λ_1 , the squared expansion coefficients of the eigenvector $v_{1,j}^2$ associated with λ_1 , the Shannon entropy of the squared eigenvector component, defined by $H(\mathbf{v}_1^2) = -\sum_{j=1}^N v_{1,j}^2 \ln v_{1,j}^2$, node degree k , and average path length $\langle L \rangle = \frac{1}{N(N-1)} \sum_{i=1}^N \sum_{j=i+1}^N L_{ij}$, where L_{ij} is the length of the path connecting nodes i and j .

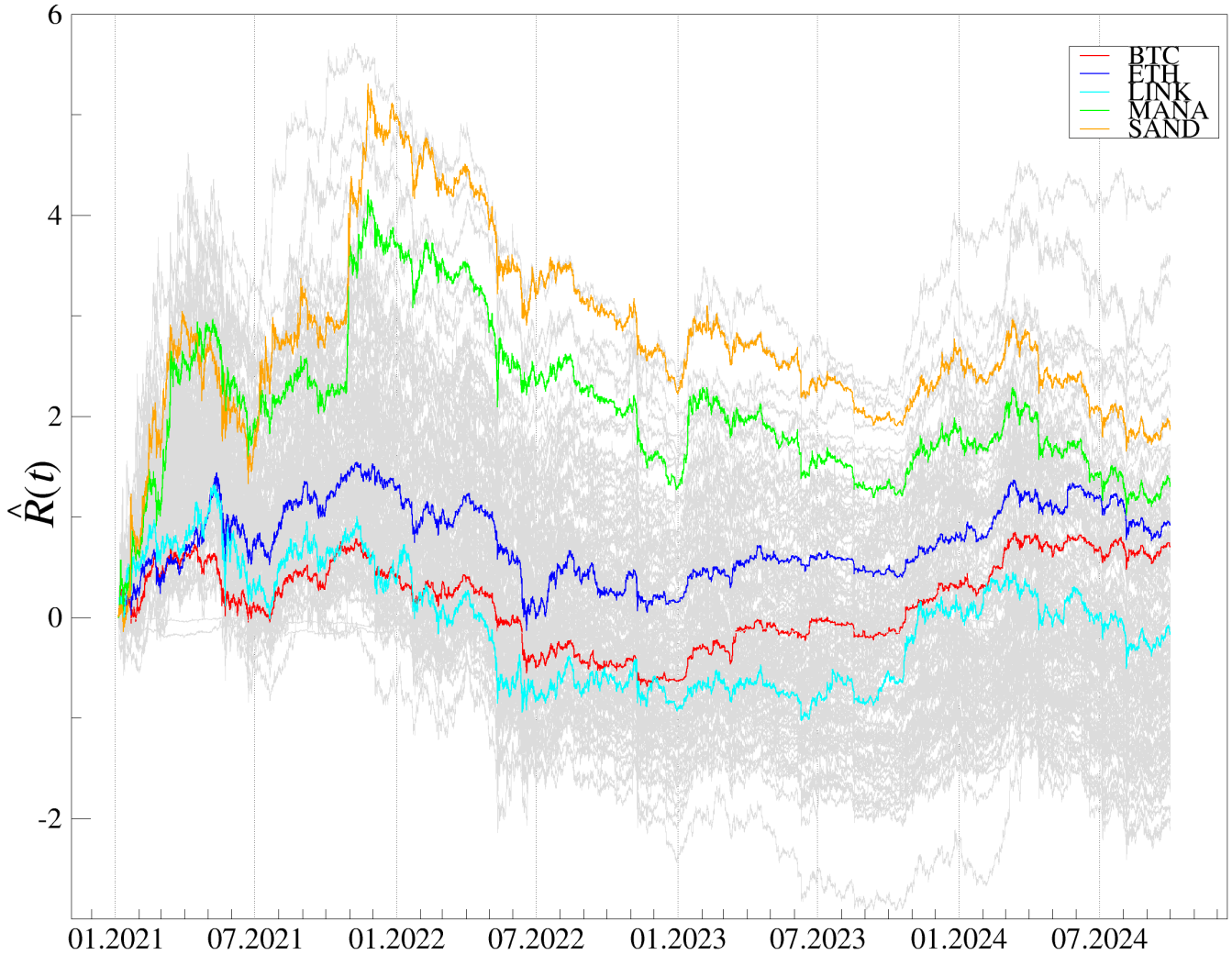


FIG. 1. Evolution of the cumulative log-returns $\hat{R}(t)$ of the 140 cryptocurrencies over the time period from Jan 1, 2021 to Sep 30, 2024. The colors of two of the most liquid cryptocurrencies and a few other distinguished ones are indicated explicitly. The bulk of the cryptocurrencies is shown in the background (grey lines).

Fig. 2 presents the changes in selected characteristics over time for the correlation matrix $\mathbf{C}(q = 1, s = 10)$, corresponding to a scenario when the average fluctuations play the most significant role, at the shortest possible time scale $s = 10\text{min}$ selected due to the sufficient length of the segment in detrending procedure (Eq. 2) [106], with the sampling frequency of 1 min. A significant shift in network characteristics is evident starting from the rolling window ending at the end of April 2022 (as indicated by a dashed line in Fig. 2). Before this date, the MST structure was more centralized, with BTC being the highest multiplicity node in most windows. This centralized structure corresponds to a low average path length $\langle L \rangle$. In contrast, since May 2022, the MST has become more decentralized with $\langle L \rangle$ almost always above 3 (Fig. 2b) and the maximum node degree never exceeding 90 (Fig. 2a). Moreover, during this later period, BTC loses its dominant role, and various cryptocurrencies, such as ADA, DOT, ETH, LINK, MANA, SAND, and VET, emerge as the largest-multiplicity nodes.

The change in the structure of the network in May 2022 is clearly visible in Fig. 3 where two sample q MSTs calculated within rolling windows at their respective endpoints are shown: (a) 25 April-2022 and (b) 18 May-2022. Each node represents a specific cryptocurrency, while each weighted edge indicates the metric distance between a pair of cryptocurrencies. In Fig. 3a, the network structure is highly centralized, with BTC serving as the clearly largest multiplicity node with $k = 112$. In Fig. 3b, the MST structure is in the process of changing to decentralized and the largest multiplicity node is ONT with $k = 33$.

The regime change in May 2022 is also evident in the spectral characteristics of the correlation matrix. Before May 2022, cross-correlations were generally stronger as indicated by larger λ_1 values (Fig. 2c), which represent the market

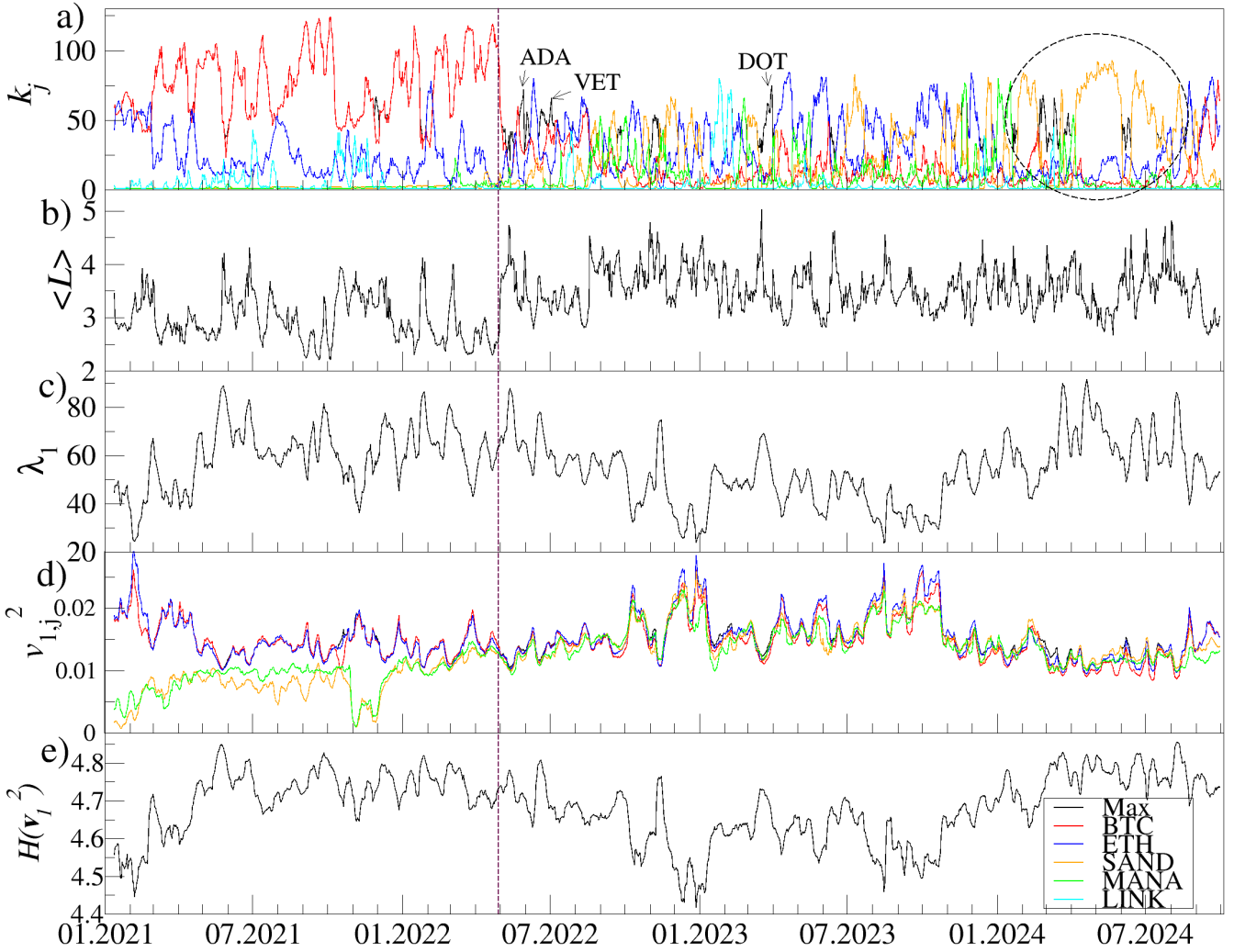


FIG. 2. Time evolution of the network characteristics of the q MSTs created from a distance matrix $\mathbf{D}(q = 1, s = 10)$: (a) node degree k_j (cryptocurrencies that had the highest multiplicity in a given window were indicated), (b) average path length $\langle L \rangle$ and spectral characteristics of the q -dependent detrended correlation matrix $\mathbf{C}(q = 1, s = 10)$: (c) the largest eigenvalue λ_1 , (d) the squared expansion coefficients of the eigenvector $v_{1,j}^2$ associated with λ_1 for $j = \text{BTC, ETH, MANA, LINK, and SAND}$ (e) the Shannon entropy $H(\mathbf{v}_1^2)$ of the squared eigenvector components. Rolling window of length 7 days shifted by 1 day was applied.

factor correlations. The diminishing dominance of BTC in the MST structure is further reflected in the reduced value of its expansion coefficient of the eigenvector $\mathbf{v}_{1,j}$ associated with λ_1 (Fig. 2d). Changes in the largest eigenvalue over time correspond to changes in the Shannon entropy of the eigenvector components associated with λ_1 (Fig. 2e). Stronger correlations (larger λ_1) indicate a more uniform share of individual cryptocurrencies in the correlations. Weaker correlation (lower λ_1) denote greater differentiation between the share of individual cryptocurrencies in the eigenvector. The observed shift in the cross-correlation structure at the end of April 2022 may be linked to the cryptocurrency market crash that developed at that time and accelerated in May 2022 following the collapse of Terra/Luna system [107].

Another interesting period can be observed from February to August 2024, where in most rolling windows, the cryptocurrency SAND, related to metaverse Sandbox became the largest multiplicity node, with $k = 90$ in some windows. This is in conjunction with an increase of λ_1 entropy values to the 2022 level. Additionally, the notable position of SAND is confirmed, as it exhibits the highest expansion coefficient values in some rolling windows at that period. At the same time, it should be noted that the highest SAND node multiplicity did not match the BTC node degree from 2021 and 2022.

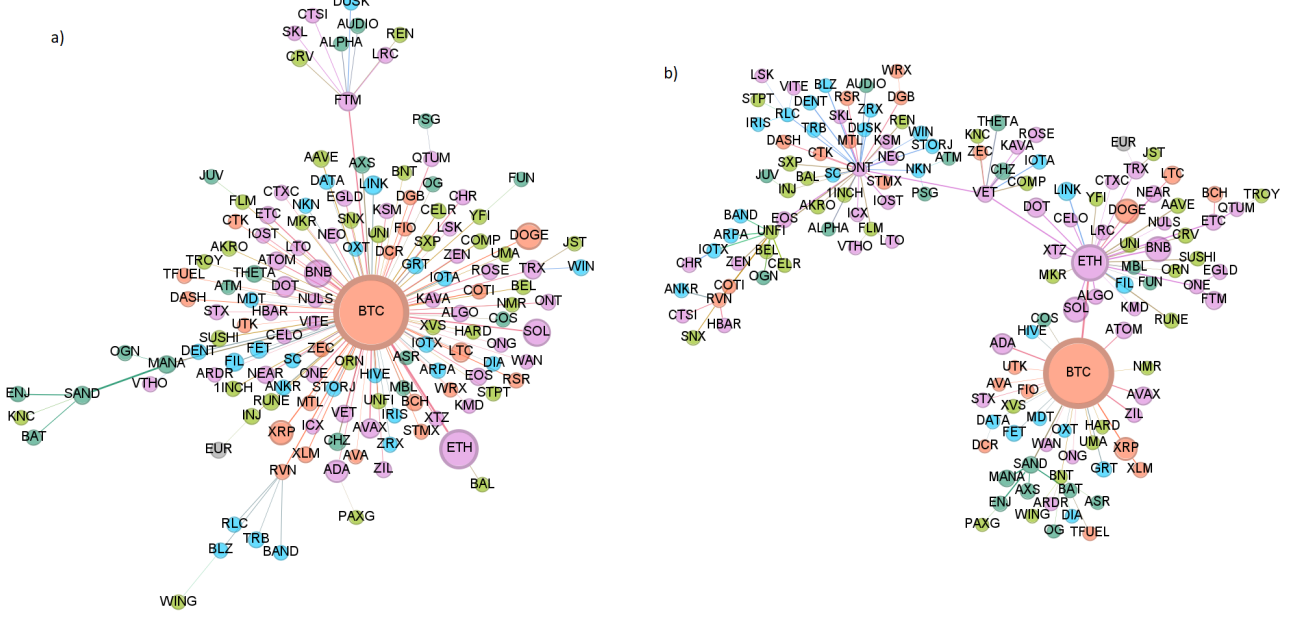


FIG. 3. Sample q MSTs calculated for ($q = 1$ and $s = 10$) in the rolling windows ending on: (a) Apr 25, 2022 and (b) May 18, 2022. Node size is proportional to the average volume in the analyzed period, while edge thickness reflects the strength of the cross-correlations. Colors represent market sectors after Digital Asset Classification Standard (DACS), created by CoinDesk [105]: currency (orange), smart contract platform (violet), computing (cyan), DeFi (green), and culture & entertainment (dark green).

B. Differences in the organization of cross-correlations at various fluctuation amplitudes

The structure of the q MST graphs looks different if the correlations between the largest fluctuations are amplified ($q = 4$). Here, the largest node degree changes significantly more often and the MST structure is less stable than in the case of $q = 1$. In Fig. 4 there is no analogous period of BTC dominance corresponding to Fig. 2. In addition, the network structure is more decentralized. This manifests itself in correlations and network characteristics presented in Fig. 5. The largest node degree is significantly lower and $\langle L \rangle$ is larger for $q = 4$ (Fig. 5a and Fig. 5b) than for $q = 1$. The differences are also visible in the spectral characteristics of the correlation matrices. The correlations measured using the largest eigenvalue λ_1 are larger for $q = 1$ than for $q = 4$ for most of the period (Fig. 5e). The largest expansion coefficient in the eigenvector associated with λ_1 is larger for $q = 4$, which indicates greater differentiation among the eigenvector components (Fig. 5f) and, thus, lower Shannon entropy of the eigenvector components associated with λ_1 for $q = 4$ (Fig. 5g).

Despite the fact that the described dependencies occur in the vast majority of windows in Fig. 5, there are a few exceptions when λ_1 values are larger for $q = 4$ than for $q = 1$. In these windows, the structure of the eigenvector expansion coefficients associated with λ_1 for $q = 4$ is homogeneous and the entropy is higher than for $q = 1$. This also affects the network structure that is fully decentralized for $q = 4$, which manifests itself through $\langle L \rangle > 10$.

To quantitatively assess when the structure of q MST differs the most depending on the parameter q , two graph distance metrics based on differences in adjacency matrices were used: DeltaCon0 denoted by d_{DC0} [108] and resistance perturbation distance denoted by d_{rp1} [109]. Their changes over time with respect to the q parameter:

$$d_{rp1}[A(q = 1, s = 10, t), A(q = 4, s = 10, t)], \quad (10)$$

$$d_{DC0}[A(q = 1, s = 10, t), A(q = 4, s = 10, t)], \quad (11)$$

where A is the adjacency matrix for a given MST tree, are presented in Fig. 5c and Fig. 5d. It turns out that the largest values of the distance metrics can be observed in the rolling windows when the network and correlation characteristics behave as in the exceptions described above, namely when stronger correlations occur at the level of large fluctuations ($q = 4$) than at the level of average fluctuations ($q = 1$). These rolling windows are marked by dotted lines in Fig. 5. The explanation behind such situations is the price collapse of almost all cryptocurrencies within a few minutes. The trajectories of the price changes in the sample rolling windows when such a crash occurred

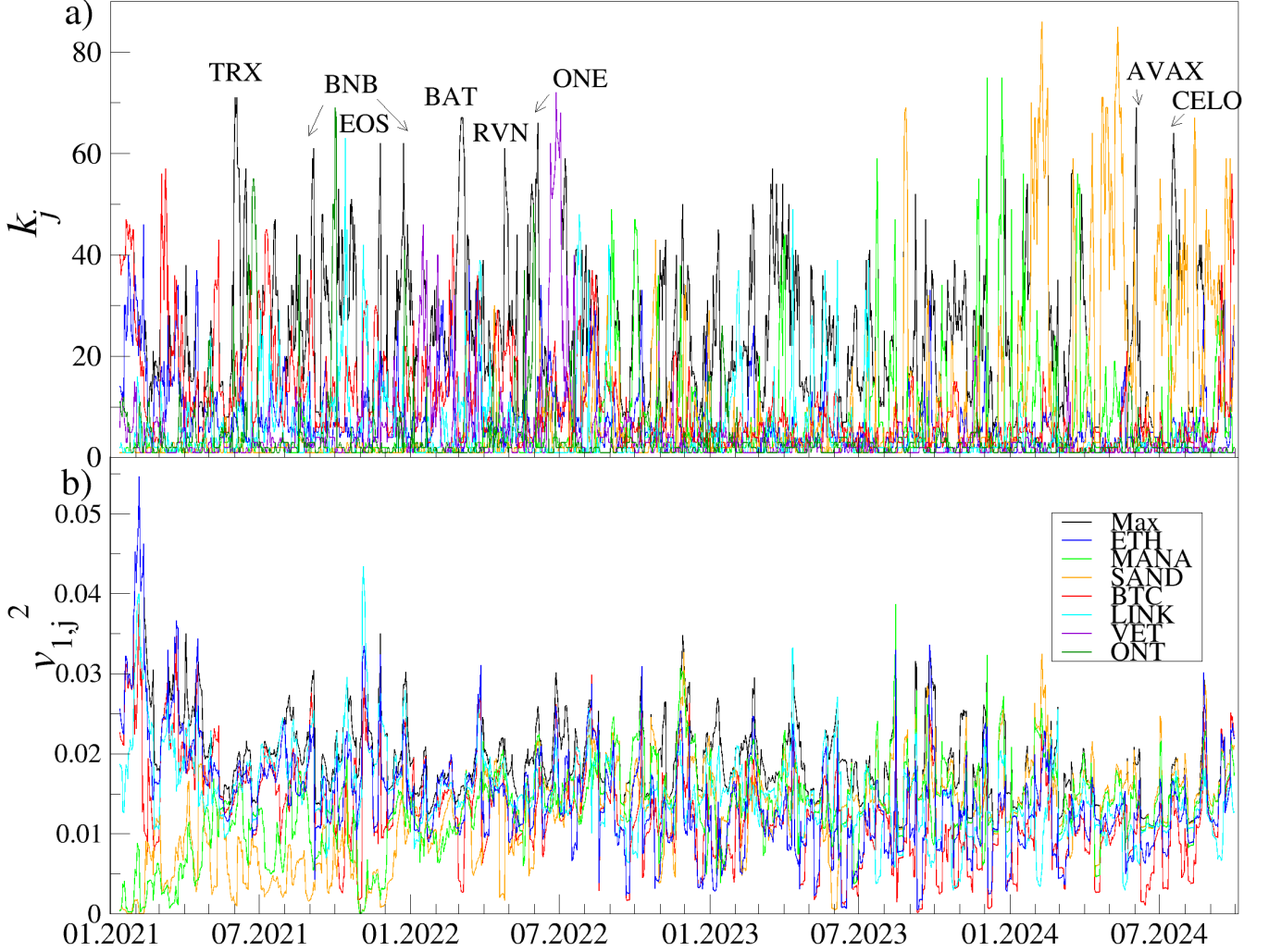


FIG. 4. Time evolution of the network characteristics of the q MSTs created from a distance matrix $\mathbf{D}(q = 4, s = 10)$: (a) node degree k_j (cryptocurrencies that had the largest multiplicity in a given window were indicated) and spectral characteristics of the q -dependent detrended correlation matrix $\mathbf{C}(q = 4, s = 10)$: (b) the squared expansion coefficients of the eigenvector $\mathbf{v}_{1,j}^2$ associated with λ_1 for $j = \text{BTC, ETH, SAND, MANA, and LINK}$.

(marked by Roman numerals in 5) are presented in Fig. 6. There is a visible drop in all exchange rates.

The q MSTs obtained from the date range presented in Fig. 6, when the rolling windows contain crashes marked by (a) and (b) and when the crashes exceed the weekly data range marked by (c) and (d) are presented in Fig. 7, Fig. 8, and Fig. 9. It is clearly visible that the structure of q MST for $q = 4$ is entirely decentralized in the windows containing the crash, and this is not the case for $q = 1$ ((a) and (b) in Figs. 7 and 8). On the other hand, when there is no crash in a rolling window from which the q MST was obtained, the graph structure for both values of q is similar ((c) and (d) in Figs. 7 and 8). Such behaviour is related to the fact that, for $q = 4$, the role of large fluctuations is amplified in $\rho_q(s)$, leading to stronger cross-correlations during crashes, when such large fluctuations occur. This is reflected in larger λ_1 , homogeneous behaviour of the expansion coefficients, and complete decentralization of the q MST structure for $q = 4$, because everything is strongly cross-correlated and thus behave in the same way. This effect is weaker for $q = 1$, where large fluctuations are not amplified. These examples demonstrate the usefulness of the q MST methodology in capturing subtleties of correlation behaviour.

Another observation is that the largest differences between graph structures for $q = 1$ and $q = 4$ used to occur mainly from mid-2023 to mid-2024. It indicates that the cryptocurrency market became more unstable at that time.

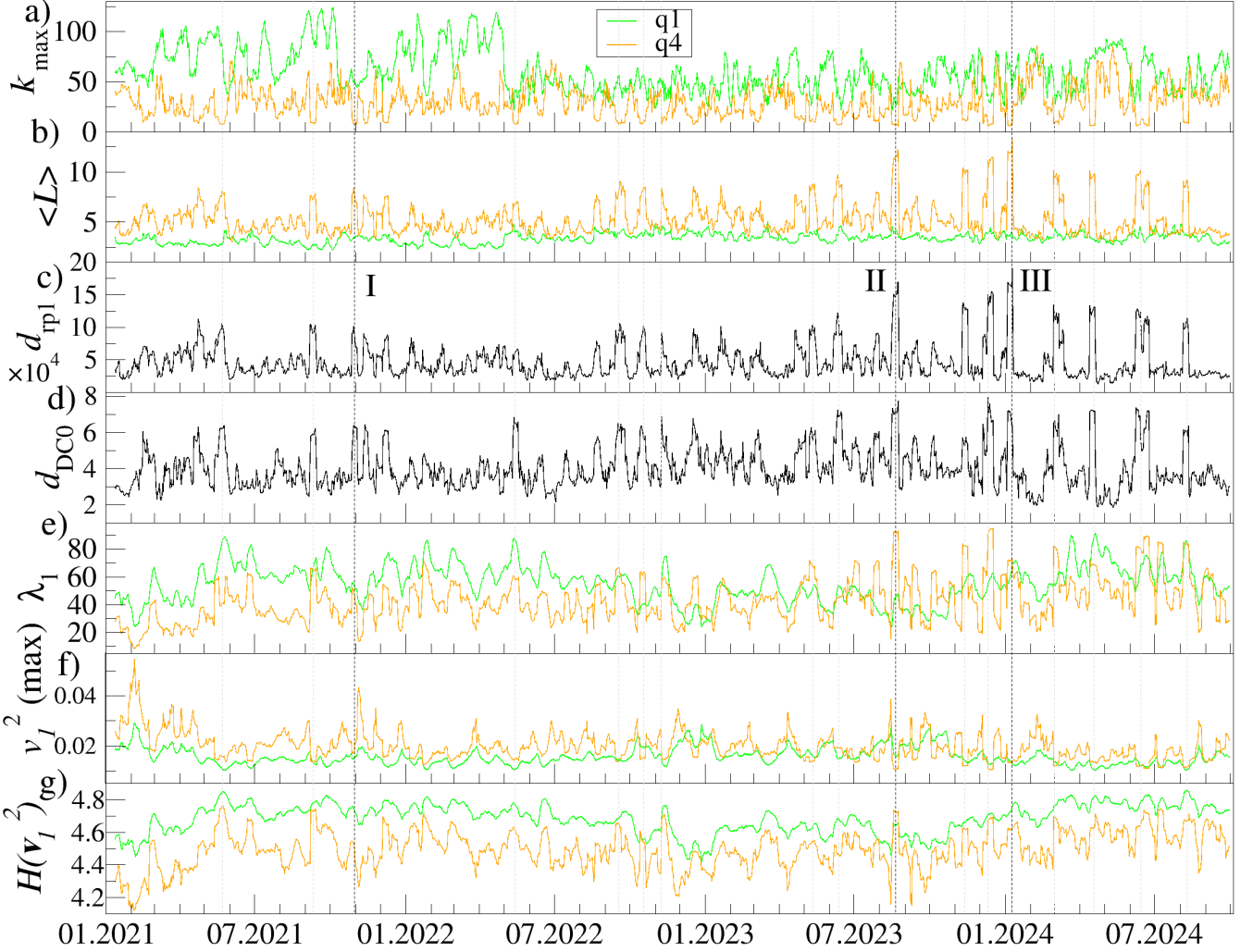


FIG. 5. Time evolution of the network characteristics of the q MSTs created from a distance matrix $\mathbf{D}(q = 1, s = 10)$ and $\mathbf{D}(q = 4, s = 10)$: (a) max node degree k_{\max} , (b) average path length $\langle L \rangle$, (c) d_{rp1} , and (d) d_{DC0} between $q = 1$ and $q = 4$ MST. The spectral characteristics of the q -dependent detrended correlation matrix $\mathbf{C}(q = 1, s = 10)$ and $\mathbf{C}(q = 4, s = 10)$: (e) the largest eigenvalue λ_1 , (f) the highest squared expansion coefficients of the eigenvector $\mathbf{v}_{1,\max}^2$ associated with λ_1 , and (g) the Shannon entropy $H(\mathbf{v}_1^2)$ of the squared eigenvector components. Rolling window of length 7 days shifted by 1 day was applied. Periods with large intraday drops are marked with Roman numerals and dotted lines.

C. Filtered correlation matrices and the corresponding q MSTs

In Sect. III B, it was observed that during certain periods, the whole market was moving in the same direction. It was visible in an increase in the value of λ_1 , which represents the so-called market factor, and the equal share of all cryptocurrencies in the eigenvector corresponding to it. This led to a reduction in the role of out-of-trend cross-correlations. To extract information about them, it is necessary to filter out the variance contribution associated with λ_1 . This can be done by using a regression-based method [69, 110]:

$$c_{\Delta t}^{(i)}(k) = a^{(i)} + b^{(i)} Z_1(k) + \epsilon^{(i)}(k),$$

$$Z_1(k) = \sum_{m=1}^N v_{1m} c_{\Delta t}^{(m)}(k), \quad (12)$$

where $Z_1(k)$ is the contribution to total variance associated with λ_1 ($k = 1, \dots, T$) and the filtered matrix \mathbf{C}' is constructed from the residual time series $\epsilon^{(i)}(k)$ ($i = 1, \dots, N$). It can be diagonalized by solving the problem $\mathbf{C}' \mathbf{v}'_i = \lambda'_i \mathbf{v}'_i$. In this subsection, the spectral properties of the residual matrix \mathbf{C}' and the network properties of the corresponding

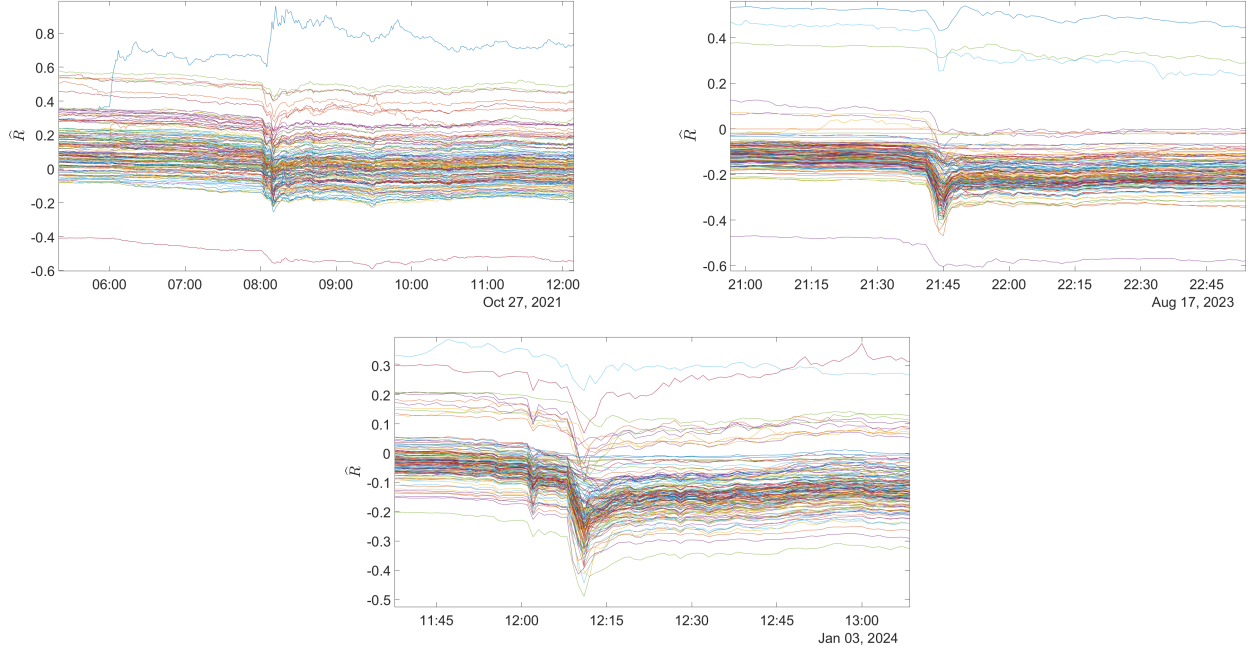


FIG. 6. Cumulative log-returns $\hat{R}(t)$ occurring during sample periods with large intraday drops corresponding to large difference between q MSTs for $q = 1$ and $q = 4$ presented in Figs. 7, 8, and 9.

q MST will be investigated in full analogy to the complete matrix \mathbf{C} in Sect. III A. The first, quite obvious observation is that the cross-correlations measured with the largest eigenvalue of the filtered correlation matrix λ'_1 are weaker in all rolling windows for both values of q - see Fig. 10e. Also, the maximum node degree presented in Fig. 10a is significantly smaller after correlation filtering. This results in a more decentralized structure in most windows, indicated by larger $\langle L \rangle$ in Fig. 10b. There is also no outlier of $\langle L \rangle$ observed unlike Fig. 5b. The smaller variation in the characteristics of the q MST characteristics with respect to q translates into smaller values of the graph distance metrics in Fig. 10c and Fig. 10d. On the other hand, in the case of filtered correlations, there are significantly larger maximum values of the eigenvector expansion coefficient (Fig. 10f), which corresponds to smaller values of the expansion coefficient entropy (Fig. 10g) and, thus, their greater diversity, especially in large fluctuations ($q = 4$). However, this takes place with much weaker correlations (smaller λ'_1). Therefore, this does not translate itself into the structure of q MSTs.

The filtering procedure has also affected the nodes with the largest multiplicity in q MSTs. For both $q = 1$ (Fig. 11a) and $q = 4$ (Fig. 11c) BTC is visible as the most connected node in 2021 until mid-2022. This effect is weaker than in the case of unfiltered correlations for $q = 1$ in Fig. 2a, however. On the other hand, BTC is visible as the most connected node until mid-2022 for $q = 4$, which was not the case before the correlation filtering. The second difference is the absence of SAND as the node with the largest multiplicity in 2024 for both values of q (Fig. 11a and Fig. 10b). In the case of the filtered correlations, it does not play a dominant role. It means that the appearance of SAND in 2024 as the most connected node for both values of q was related to the market factor, and after filtering it out, the effect disappeared. However, the dominant role of BTC and ETH is still visible after filtering out the market factor (Fig. 11), which suggests that their role in the market correlation structure is more durable.

D. Dependencies between correlation and distance matrices measures

In the previous sections, the changes in the network and spectral characteristics were analyzed in rolling windows. As it can be seen from the results, the considered measures depend on each other. In order to verify quantitatively to what extent the correlations between the time series constructed from the values of the previously analyzed characteristics in each window position ($k = 1, \dots, K$, $K = 1357$ windows) were calculated using the Pearson coefficient. The results for each of the variants previously considered are presented in Fig. 12: (a) $\mathbf{C}(q = 1, s = 10)$, (b) $\mathbf{C}(q = 4, s = 10)$, (c) $\mathbf{C}'(q = 1, s = 10)$, and (d) $\mathbf{C}'(q = 4, s = 10)$.

The strongest cross-correlations occur in the group of the spectral characteristics of the correlation matrix: λ_1 ,

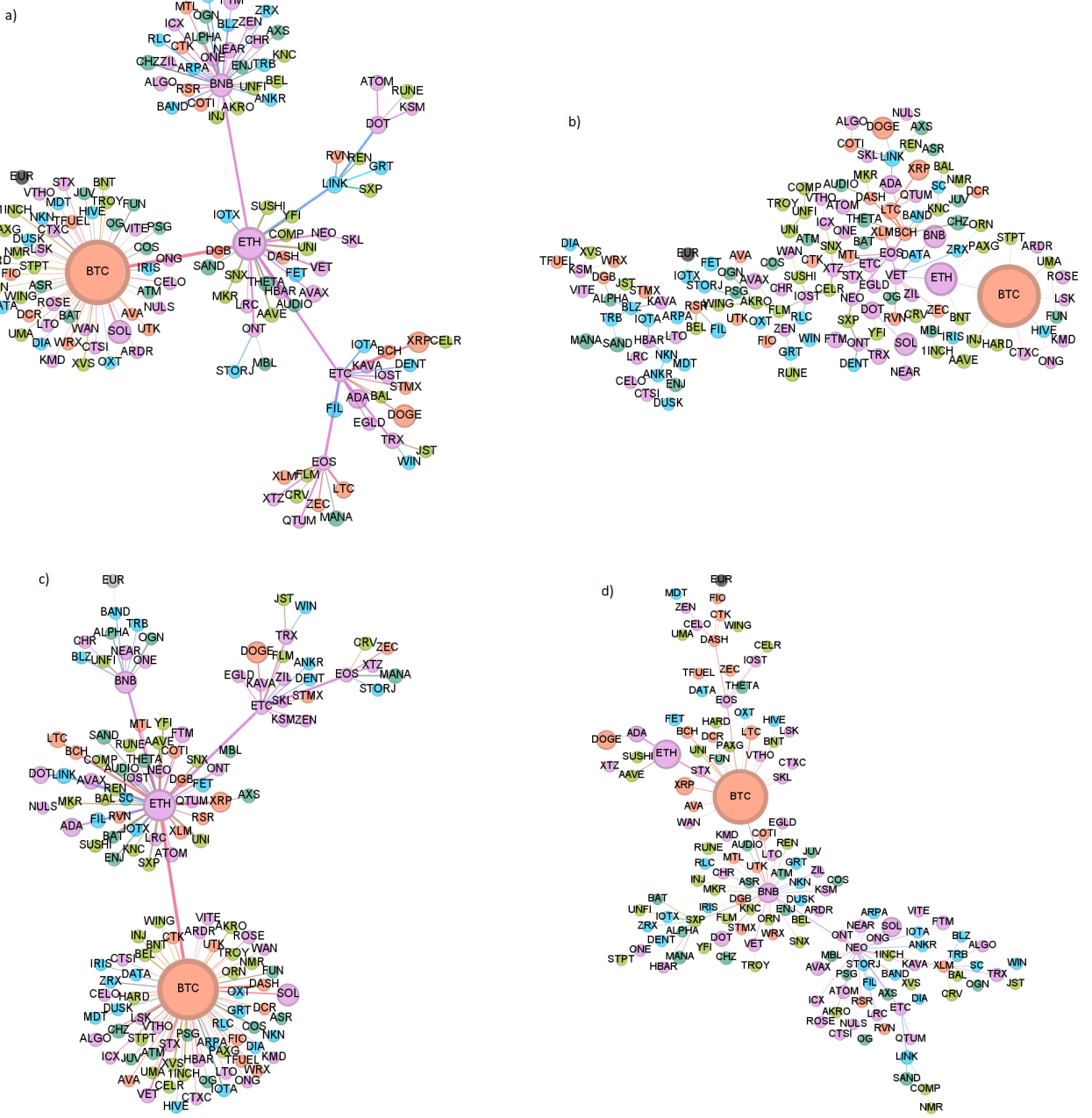


FIG. 7. q MST's calculated in a rolling window when the metrics d_{DC0} and d_{rp1} for $q = 1$ (left - a and c) and $q = 4$ (right - b and d) were among the largest: the window ending on Oct 30, 2021 (upper - a and b) and the window ending on Oct 26, 2021 (lower - c and d); these windows correspond to crashes falling out of the weekly data range.

\mathbf{v}_1^2 , $H(\mathbf{v}_1^2)$ and in the group of the network characteristics: $\langle L \rangle$ and k_{\max} . They assume the highest values for medium-amplitude fluctuations ($q = 1$), with their values even higher than for large fluctuations ($q = 4$). The cross-correlations are correspondingly weaker after filtering out the variance associated with λ_1 (bottom panels in Fig. 12). In contrast, the cross-correlations between the metrics belonging to different groups are weak. However, in the case of large fluctuations, significant cross-correlation also occurs between the spectral characteristics of the correlation matrix and the network characteristics of q MSTs (Fig. 5b). The largest (≈ 0.6) is observed for $\langle L \rangle$ and λ_1 . It is related to the appearance of sudden jumps in the cross-correlation level as measured by λ_1 during crashes, which influenced all the other characteristics for $q = 4$ (the cases marked in Fig. 5).

The cross-correlations of the analyzed characteristics seem natural due to the fact that they are based on the

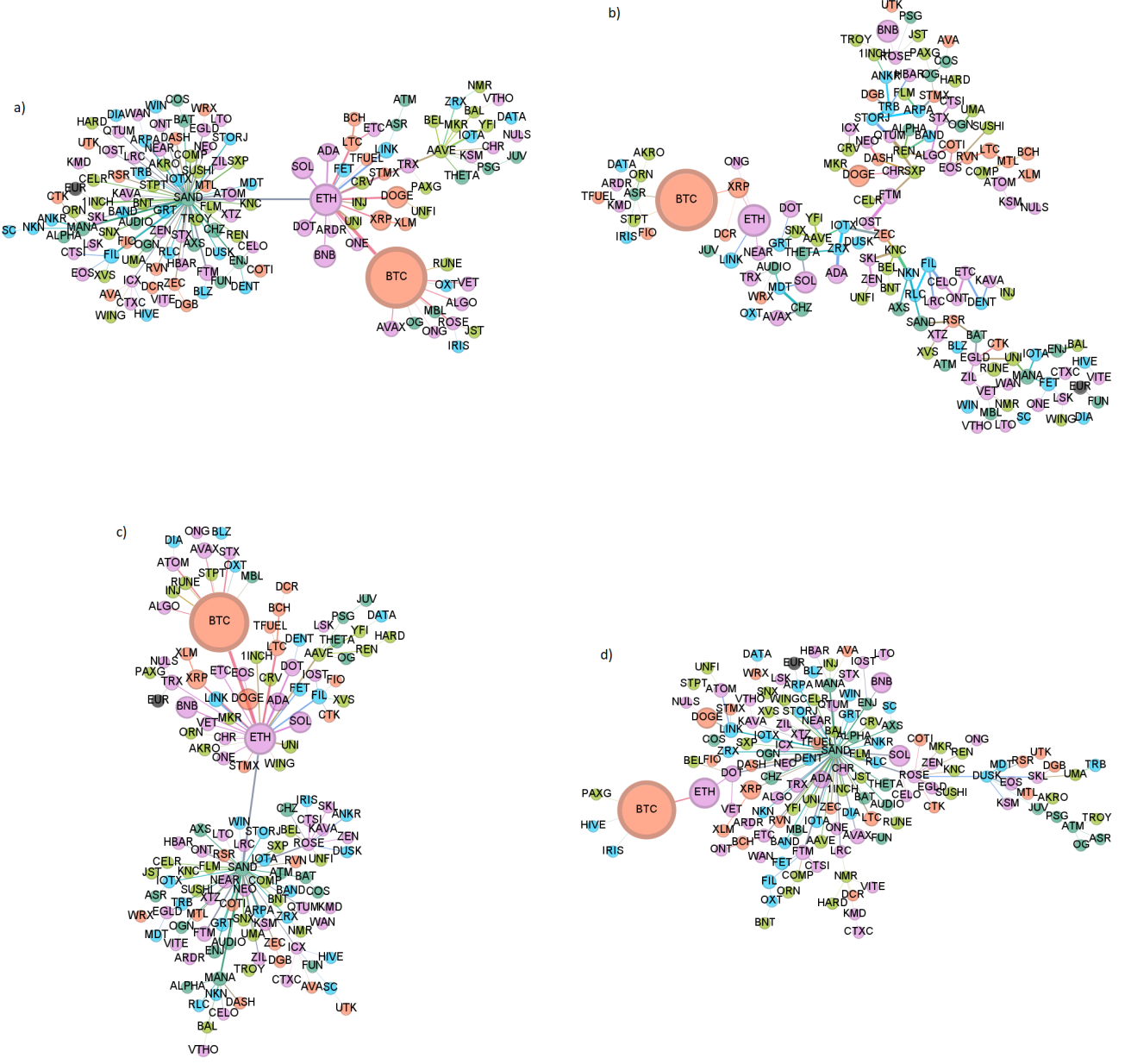


FIG. 8. q MSTs in rolling window when the metrics d_{DC0} and d_{rp1} for $q = 1$ (left - a and c) and $q = 4$ (right - b and d) were one of the largest: the window ending on Aug 24, 2023 (upper - a and b) and the window ending on Aug 5, 2023 (lower - c and d) when the crashes led to the market falling out of the weekly data range.

same correlation matrices and the q MSTs, but it turns out that all the considered metrics are also characterized by long-range autocorrelation, defined as

$$A(x, \Delta k) = \frac{\frac{1}{K} \sum_{k=1}^K [x(k) - \langle x(k) \rangle_i] [x(k + \Delta k) - \langle x(k) \rangle_k]}{\sigma_x^2}, \quad (13)$$

where σ_x is the estimated standard deviation of the time series $x(k)$, $\langle \cdot \rangle$ represents the estimated mean, and Δk is the time lag in terms of rolling windows. Significant autocorrelations exceeded the obvious range of $\Delta k = 6$ days, which resulted from a data overlap in 7-day windows - see Fig 13. The longest autocorrelation range occurred for the

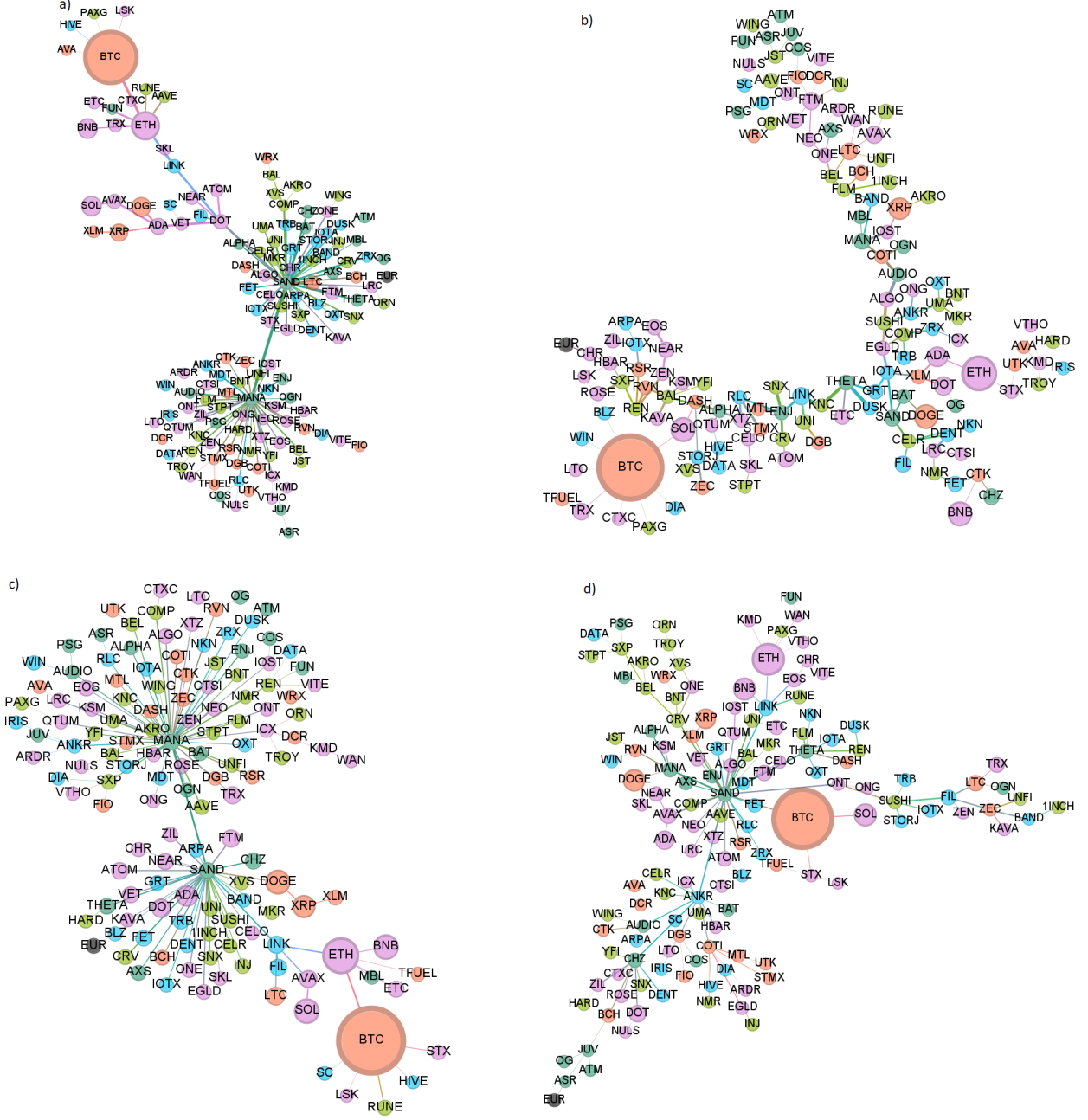


FIG. 9. q MSTs in rolling window when the metrics d_{DC0} and d_{rp1} for $q = 1$ (left - a and c) and $q = 4$ (right - b and d) were one of the largest: the window ending on Jan 10, 2024 (upper - a and b) and the window ending on Jan 11, 2024 (lower - c and d) when the crashes led to the market falling out of the weekly data range.

characteristics obtained for the unfiltered matrix $\mathbf{C}(q = 1, s = 10)$: $\Delta k \approx 150$ in the case of the spectral measures λ_1 , $\mathbf{v}_{1,\max}^2$, $H(\mathbf{v}_1^2)$ and $\Delta k \approx 250$ in the case of the network measures $\langle L \rangle$ and k_{\max} (Fig 13a). For $q = 4$ and after filtering out the influence of the largest eigenvalue, the autocorrelation range is shorter but still significant.

Such behavior of the considered measures can be explained by a power-law decay of the volatility autocorrelation function, which is one of the stylized facts observed on all financial markets [111–113]. An interesting related fact is that the length of the power law decay in the measures is comparable with the power law decay of the ACF in the case of BTC and ETH volatility [114]. The mechanism behind it is the volatility increase because larger volatility usually results in stronger correlations, which may have an impact on the spectral and network measures, as it was shown in the previous subsections.

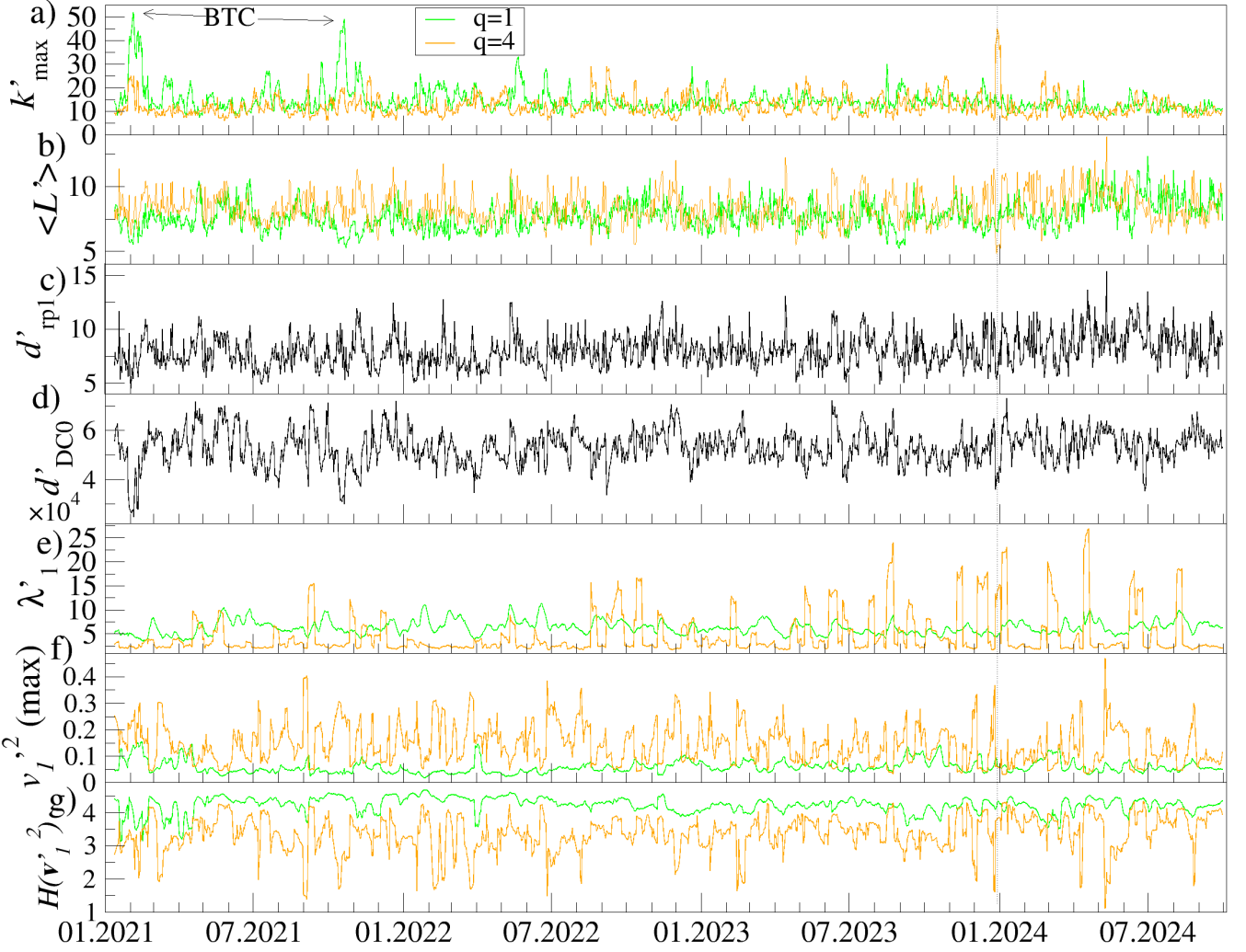


FIG. 10. The same measures as in Fig.5, but for the filtered correlation matrix \mathbf{C}' .

IV. CONCLUSION

This work studied the detrended cross-correlation structure of the cryptocurrency market using the q MST approach. In particular, it was investigated how this structure changes over time, depending on the range of fluctuation amplitude. It turned out that since May 2022, there has been a significant change in the structure of the q MST's. Bitcoin has ceased to be its central node, and other cryptocurrencies have taken over this role. At the same time, the q MST's have become more decentralized. An important part of this analysis was the identification of the dependence of the topology of q MST on the fluctuation amplitude. Medium-size fluctuations are more strongly cross-correlated with each other than large fluctuations. Consequently, the q MST graphs created from the correlation matrices with the amplified role of the largest fluctuations are more decentralized than their counterparts created from the correlation matrices with the dominant role of medium fluctuations. Moreover, the quantitative analysis of the difference between the individual cross-correlation networks depending on the fluctuation amplitude of the considered fluctuations was carried out using distance graph measures. It showed that the greatest differences occur at the time of large market events like crashes on most cryptocurrencies. During such events, the largest fluctuations were more strongly cross-correlated with each other and the q MST's structure were completely decentralized if these fluctuations were amplified by applying $q = 4$. In the case of a focus on medium-size fluctuations with $q = 2$, the graph structure was more centralized. Another general observation was that, generally, the network was becoming less centralized with increasing cross-correlation strength.

The study reported in this work illustrates the usefulness of the q MST concept, which allows for the selection of the fluctuation amplitude range in a network of interacting elements like assets in the financial markets. The

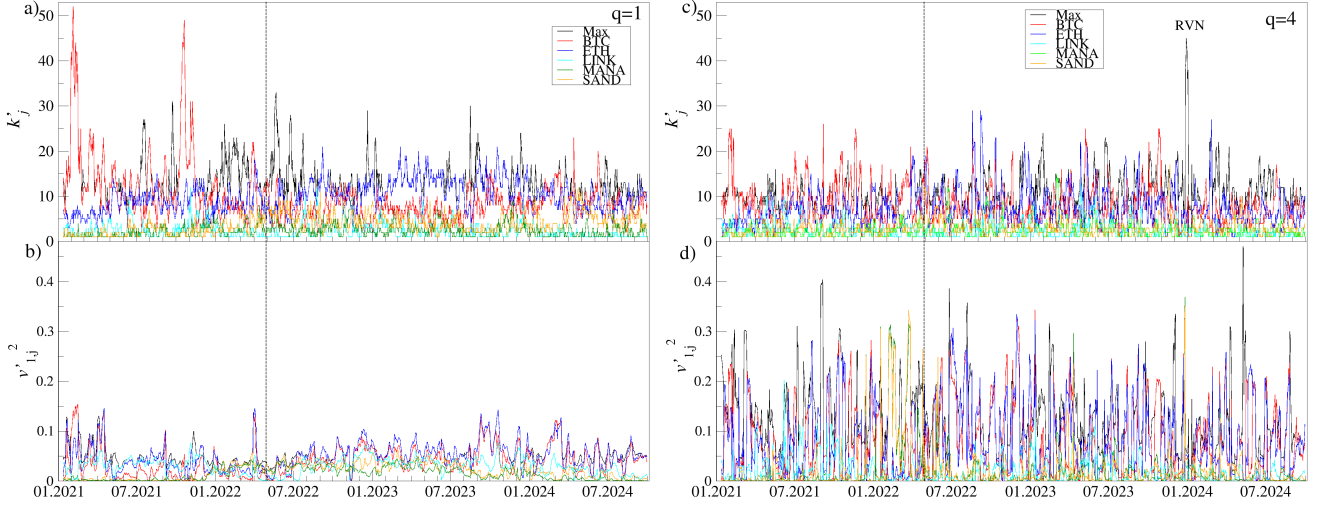


FIG. 11. Time evolution of the network characteristics of the q MSTs created from the filtered distance matrices $\mathbf{D}'(q = 1, s = 10)$ (left) and $\mathbf{D}'(q = 4, s = 10)$ (right): (a) node degree k_j (cryptocurrencies that had the largest node degree in a given window were indicated) and the spectral characteristics of the q -dependent detrended filtered correlation matrix $\mathbf{C}'(q = 1, s = 10)$ (left) and $\mathbf{C}'(q = 4, s = 10)$ (right); (b) the squared expansion coefficients of the eigenvector $\mathbf{v}'_{1,j}^2$ associated with λ'_1 for $j = \text{BTC, ETH, SAND, MANA, and LINK}$.

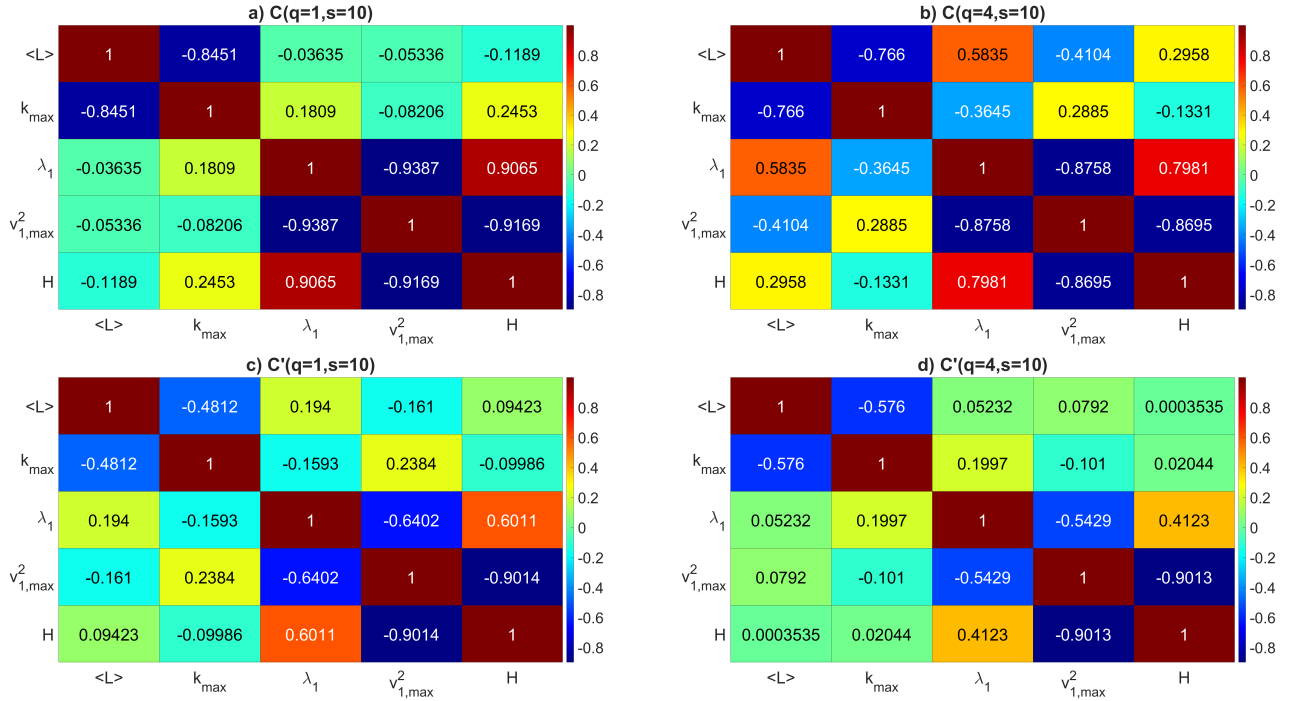


FIG. 12. Correlation between the spectral measures λ_1 , $v_{1,\max}^2$, $H(v_1^2)$ and the network measures $\langle L \rangle$ and k_{\max} obtained from: (a) $C(q = 1, s = 10)$, (b) $C(q = 4, s = 10)$, (c) $C'(q = 1, s = 10)$, and (d) $C'(q = 4, s = 10)$.

effectiveness of this methodology was illustrated here by the example of the cryptocurrency market and the conclusions regarding its cross-correlation structure that were drawn. This may introduce novel elements for constructing optimal portfolios. The discussed spectral and network characteristics can be monitored in real time, thus the investor can use different strategies depending on the degree of correlations at the level of different fluctuations, and also detect the connections between individual cryptocurrencies and the emerging sectors in MST trees. For example, this information may support portfolio managers in applying allocation strategies: portfolios emphasizing medium-scale fluctuations would reflect stronger cross-asset correlations and thus require greater diversification to mitigate systemic risk, while

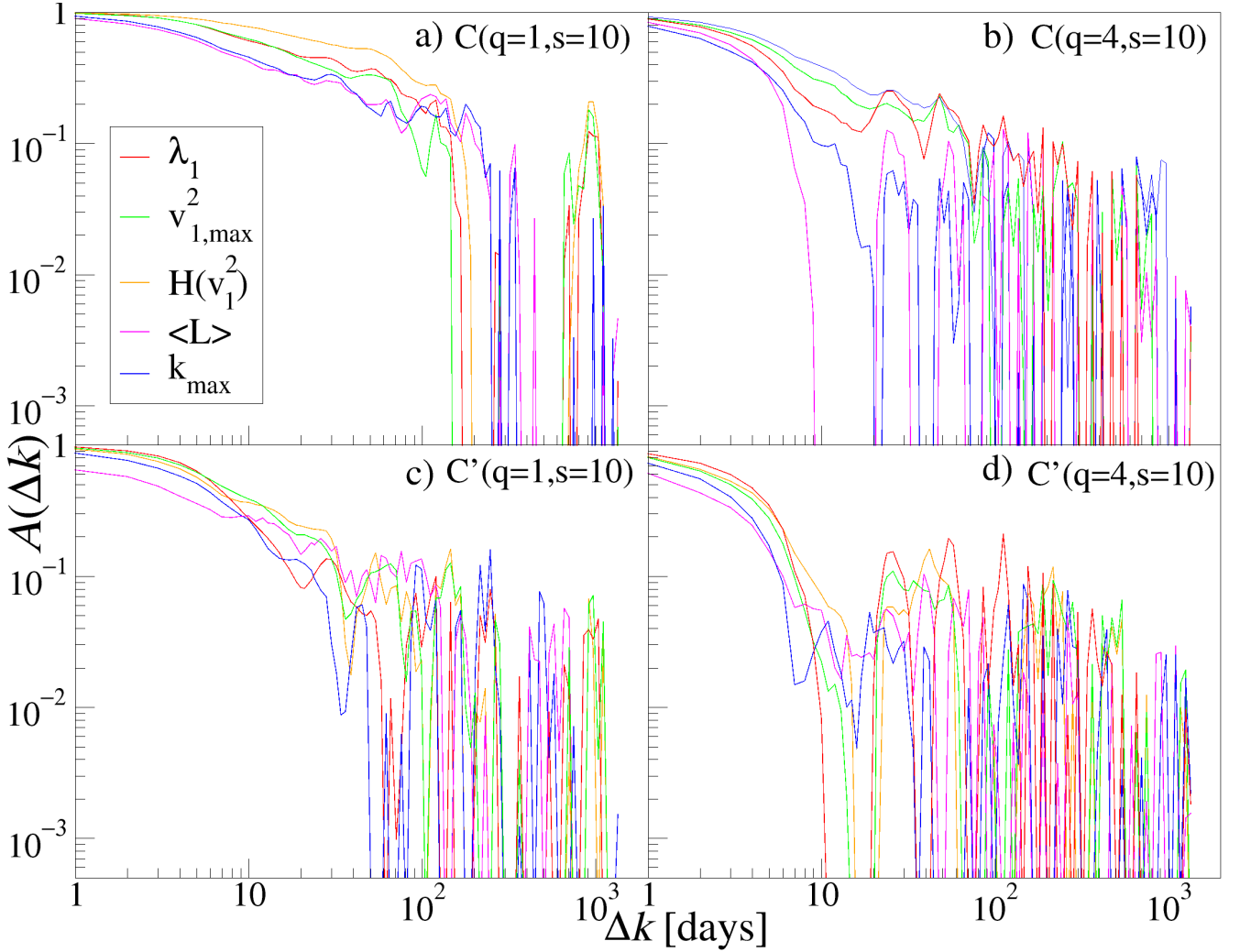


FIG. 13. Autocorrelation functions for λ_1 , $v_{1,\max}^2$, $H(v_1^2)$, $\langle L \rangle$, and k_{\max} obtained from: (a) $C(q = 1, s = 10)$, (b) $C(q = 4, s = 10)$, (c) $C'(q = 1, s = 10)$, and (d) $C'(q = 4, s = 10)$.

portfolios constructed on large-scale fluctuations may benefit from more decentralized structures that highlight sector-specific clusters. Such insight may also be used at rebalancing time to down-weight crypto assets in the portfolio that are known to be vulnerable. In this way, q MST-based analysis can extend the traditional correlation-based methods by tailoring allocation, hedging, and risk management strategies to fluctuation-specific correlation patterns. The specific use of the described dependencies in portfolio management thus emerges an inspiring issue and a promising direction for future studies. Finally, from a more general perspective, it should be noted that the same methodology can successfully be applied to many other natural and human-made complex systems.

ACKNOWLEDGMENTS

The research was funded by National Science Centre, Poland, grant number 2023/07/X/ST6/01569. The authors MC and MB wish to acknowledge the support from the Science Foundation Ireland under Grant Agreement No. 13/RC/2106_P2 at the Research Ireland Centre at DCU. , the Research Ireland Centre for AI Driven Digital Content Technology, is funded by Research Ireland (URL: <https://www.centre.ie/>).

Appendix A: List of the tickers

TABLE I: Full list of the cryptocurrencies considered in this study, with the basics statistics - average volume value $\langle V_{\Delta t} \rangle$, the average number of transaction $\langle N_{\Delta t} \rangle$ and fraction of zero log-returns $\%0R_{\Delta t}$ for $\Delta t=1\text{min}$. The classification into a given sector was made on the basis of Digital Asset Classification Standard (DACS), created by CoinDesk [105].

Ticker	Name	Sector	$\langle V_{\Delta t} \rangle$	$\langle N_{\Delta t} \rangle$	$\%0R_{\Delta t}$
IINCH	1inch Network	DeFi	12353	45	0.27
AAVE	Aave	DeFi	23580	71	0.20
ADA	Cardano	Smart Contract Platform	147855	232	0.16
AKRO	Akropolis	DeFi	3669	31	0.37
ALGO	Algorand	Smart Contract Platform	21057	71	0.20
ALPHA	Stella	Culture & Entertainment	7648	25	0.32
ANKR	Ankr network	Computing	10567	37	0.19
ARDR	Ardor	Smart Contract Platform	1475	9	0.55
ARPA	ARPA	Computing	6702	33	0.17
ASR	AS Roma Fan Token	Culture & Entertainment	1730	11	0.47
ATM	Atletico Madrid Fan Token	Culture & Entertainment	2589	12	0.52
ATOM	Cosmos	Smart Contract Platform	38781	106	0.09
AUDIO	Audius	Culture & Entertainment	7784	29	0.32
AVA	Travala.com	Currency	1402	10	0.51
AVAX	Avalanche	Smart Contract Platform	78335	150	0.17
AXS	Axie Infinity	Culture & Entertainment	36413	72	0.25
BAL	Balancer	DeFi	2380	11	0.34
BAND	Band Protocol	Computing	5845	24	0.26
BAT	Basic Attention Token	Culture & Entertainment	8332	35	0.23
BCH	Bitcoin Cash	Currency	39413	73	0.23
BEL	Bella Protocol	DeFi	4741	26	0.26
BLZ	Bluzelle	Computing	5690	28	0.30
BNB	BNB	Smart Contract Platform	271516	360	0.19
BNT	Bancor	DeFi	2281	13	0.41
BTC	Bitcoin	Currency	1955792	1693	0.02
CELO	Celo	Smart Contract Platform	8410	30	0.33
CELR	Celer Network	DeFi	9515	33	0.25
CHR	Chromia	Smart Contract Platform	14296	45	0.25
CHZ	Chiliz	Culture & Entertainment	45331	97	0.23
COMP	Compound	DeFi	8763	33	0.17
COS	Contentos	Culture & Entertainment	3960	25	0.44
COTI	COTI	Currency	10442	42	0.25
CRV	Curve DAO Token	DeFi	22169	66	0.24
CTK	Shentu	Currency	3219	22	0.38
CTSI	Cartesi	Smart Contract Platform	7055	24	0.30
CTXC	Cortex	Smart Contract Platform	4408	25	0.37
DASH	Dash	Currency	10883	34	0.24
DATA	Streamr	Computing	3840	22	0.38
DCR	Decred	Currency	970	8	0.56
DENT	Dent	Computing	13852	40	0.35
DGB	DigiByte	Currency	3325	16	0.39
DIA	DIA	Computing	2466	13	0.46
DOGE	Dogecoin	Currency	243222	345	0.11
DOT	Polkadot	Smart Contract Platform	105383	179	0.16
DUSK	Dusk Network	Computing	4595	25	0.33
EGLD	MultiversX	Smart Contract Platform	18389	53	0.13
ENJ	Enjin Coin	Culture & Entertainment	17924	51	0.21
EOS	EOS	Smart Contract Platform	44207	87	0.28
ETC	Ethereum Classic	Smart Contract Platform	54983	90	0.21
ETH	Ethereum	Smart Contract Platform	910432	697	0.02
EUR	Euro	fiat currency	31981	59	0.49
FET	Fetch.ai	Computing	20467	78	0.19
FIL	Filecoin	Computing	62813	116	0.17
FIO	FIO Protocol	Currency	2186	12	0.51
FLM	Flamingo Finance	DeFi	4576	19	0.38

Ticker	Name	Sector	$\langle V_{\Delta t} \rangle$	$\langle N_{\Delta t} \rangle$	$\%0R_{\Delta t}$
FTM	Fantom	Smart Contract Platform	64938	138	0.10
FUN	FUNToken	Culture & Entertainment	2751	17	0.44
GRT	The Graph	Computing	20158	67	0.22
HARD	Kava Lend	DeFi	3497	16	0.39
HBAR	Hedera	Smart Contract Platform	13672	43	0.34
HIVE	Hive	Computing	2724	13	0.36
ICX	ICON	Smart Contract Platform	5939	22	0.34
INJ	Injective	DeFi	14880	51	0.18
IOST	IOST	Smart Contract Platform	11289	34	0.37
IOTA	IOTA	Computing	10770	39	0.22
IOTX	IoTeX	Computing	11136	44	0.20
IRIS	IRISnet	Computing	2147	14	0.41
JST	JUST	DeFi	5775	15	0.34
JUV	Juventus	Culture & Entertainment	1871	11	0.53
KAVA	Kava	Smart Contract Platform	11703	38	0.26
KMD	Komodo	Smart Contract Platform	1774	14	0.44
KNC	Kyber Network Crystal	DeFi	5410	22	0.35
KSM	Kusama	Smart Contract Platform	10838	38	0.23
LINK	Chainlink	Computing	69537	138	0.12
LRC	Loopring	Smart Contract Platform	17362	51	0.19
LSK	Lisk	Smart Contract Platform	2792	13	0.50
LTC	Litecoin	Currency	70616	142	0.13
LTO	LTO Network	Smart Contract Platform	2728	17	0.46
MANA	Decentraland	Culture & Entertainment	38854	106	0.11
MBL	MovieBloc	Culture & Entertainment	3761	19	0.37
MDT	Measurable Data	Computing	4015	26	0.30
MKR	Maker	DeFi	8498	25	0.33
MTL	Metal	Currency	5867	24	0.37
NEAR	NEAR Protocol	Smart Contract Platform	45831	105	0.14
NEO	Neo	Smart Contract Platform	15854	40	0.33
NKN	NKN	Computing	5494	21	0.39
NMR	Numeraire	DeFi	2383	14	0.46
NULS	Nuls	Smart Contract Platform	3080	16	0.42
OGN	Origin Protocol	Culture & Entertainment	8763	33	0.28
OG	OG Fan Token	Culture & Entertainment	3573	20	0.37
ONE	Harmony	Smart Contract Platform	18757	58	0.21
ONG	Ontology Gas	Smart Contract Platform	2635	14	0.44
ONT	Ontology	Smart Contract Platform	12481	39	0.25
ORN	Orion Protocol	DeFi	2885	20	0.38
OXT	Orchid	Computing	3140	14	0.49
PAXG	PAX Gold	DeFi	2727	6	0.60
PSG	Paris Saint-Germain Fan Token	Culture & Entertainment	3724	16	0.46
QTUM	Qtum	Smart Contract Platform	10917	33	0.24
REN	Ren	DeFi	5274	23	0.18
RLC	iExec RLC	Computing	5950	24	0.29
ROSE	Oasis Network	Smart Contract Platform	14479	58	0.10
RSR	Reserve Rights	Currency	8500	38	0.22
RUNE	THORChain	DeFi	30937	71	0.18
RVN	Ravencoin	Currency	8730	34	0.21
SAND	The Sandbox	Culture & Entertainment	48390	108	0.10
SC	Siacoin	Computing	6542	28	0.38
SKL	SKALE Network	Smart Contract Platform	5869	27	0.24
SNX	Synthetix	DeFi	10370	39	0.16
SOL	Solana	Smart Contract Platform	226651	363	0.10
STMX	StormX	Currency	6224	29	0.27
STORJ	Storj	Computing	8109	34	0.19
STPT	STP Network	DeFi	2724	17	0.41
STX	Stacks	Smart Contract Platform	10473	43	0.27
SUSHI	SushiSwap	DeFi	20544	53	0.28
SXP	SXP	DeFi	22266	60	0.26

Ticker	Name	Sector	$\langle V_{\Delta t} \rangle$	$\langle N_{\Delta t} \rangle$	$\%0R_{\Delta t}$
TFUEL	Theta Fuel	Currency	8624	30	0.38
THETA	Theta Network	Culture & Entertainment	29369	84	0.29
TRB	Tellor	Computing	10161	50	0.24
TROY	TROY	DeFi	3198	19	0.35
TRX	TRON	Smart Contract Platform	62323	127	0.17
UMA	UMA	DeFi	4488	24	0.31
UNFI	Unifi Protocol DAO	DeFi	8140	37	0.13
UNI	Uniswap	DeFi	28083	72	0.19
UTK	xMoney	Currency	2576	12	0.45
VET	Vechain	Smart Contract Platform	43606	99	0.18
VITE	Vite	Smart Contract Platform	2896	15	0.43
VTHO	VeThor	Smart Contract Platform	3757	24	0.36
WAN	Wanchain	Smart Contract Platform	1563	10	0.37
WING	Wing Finance	DeFi	2929	14	0.49
WIN	WINkLink	Computing	21341	50	0.38
WRX	WazirX	Currency	6646	26	0.41
XLM	Stellar	Currency	25483	61	0.31
XRP	XRP	Currency	228128	284	0.12
XTZ	Tezos	Smart Contract Platform	13163	41	0.35
XVS	Venus	DeFi	8713	31	0.47
YFI	yearn.finance	DeFi	10597	31	0.15
ZEC	Zcash	Currency	14810	41	0.34
ZEN	Horizen	Smart Contract Platform	5913	25	0.34
ZIL	Zilliqa	Smart Contract Platform	16615	53	0.18
ZRX	0x	Computing	5651	24	0.24

[1] P. Anderson, More is different. broken symmetry and the nature of the hierarchical structure of science., *Science* **177**, 393 (1972).

[2] M. Mitchell, *Complexity: A guided tour* (Oxford university press, 2009).

[3] J. Barral and J. Peyrière, Mandelbrot's cascades: a legendary destiny, in *Benoit Mandelbrot: A Life in Many Dimensions* (World Scientific, 2015) pp. 143–172.

[4] S. Drożdż and P. Oświęcimka, Detecting and interpreting distortions in hierarchical organization of complex time series, *Physical Review E* **91**, 030902 (2015).

[5] T. Aste, Cryptocurrency market structure: connecting emotions and economics, *Digital Finance* **1**, 5 (2019).

[6] F. Schar and A. Berentsen, *Bitcoin, blockchain, and cryptoassets: A comprehensive introduction* (MIT press, 2020).

[7] S. Corbet, B. Lucey, A. Urquhart, and L. Yarovaya, Cryptocurrencies as a financial asset: A systematic analysis, *International Review of Financial Analysis* **62**, 182 (2019).

[8] M. Wątorek, S. Drożdż, J. Kwapień, L. Minati, P. Oświęcimka, and M. Stanuszek, Multiscale characteristics of the emerging global cryptocurrency market, *Physics Reports* **901**, 1 (2021).

[9] S. Corbet, Y. G. Hou, Y. Hu, C. Larkin, B. Lucey, and L. Oxley, Cryptocurrency liquidity and volatility interrelationships during the covid-19 pandemic, *Finance Research Letters* **45**, 102137 (2022).

[10] S. Drożdż, R. Gębarowski, L. Minati, P. Oświęcimka, and M. Wątorek, Bitcoin market route to maturity? evidence from return fluctuations, temporal correlations and multiscaling effects, *Chaos* **28**, 071101 (2018).

[11] S. Begušić, Z. Kostanjčar, H. E. Stanley, and B. Podobnik, Scaling properties of extreme price fluctuations in bitcoin markets, *Physica A* **510**, 400 (2018).

[12] M. Wątorek, J. Kwapień, and S. Drożdż, Financial return distributions: Past, present, and covid-19, *Entropy* **23**, 884 (2021).

[13] T. Takaishi, Statistical properties and multifractality of bitcoin, *Physica A* **506**, 507 (2018).

[14] S. Stavroyiannis, V. Babalos, S. Bekiros, S. Lahmiri, and G. S. Uddin, The high frequency multifractal properties of bitcoin, *Physica A* **520**, 62 (2019).

[15] J. Kwapień, M. Wątorek, M. Bezbradica, M. Crane, T. Tan Mai, and S. Drożdż, Analysis of inter-transaction time fluctuations in the cryptocurrency market, *Chaos* **32**, 083142 (2022).

[16] J. Kwapień, M. Wątorek, and S. Drożdż, Multifractal cross-correlations of bitcoin and ether trading characteristics in the post-covid-19 time, *Future Internet* **14**, 215 (2022).

[17] X. Brouty and M. Garcin, Fractal properties, information theory, and market efficiency, *Chaos, Solitons and Fractals* **180**, 114543 (2024).

[18] A. Sensoy, The inefficiency of bitcoin revisited: A high-frequency analysis with alternative currencies, *Finance Research Letters* **28**, 68 (2019).

[19] T. Takaishi and T. Adachi, Market efficiency, liquidity, and multifractality of bitcoin: a dynamic study, *Asia-Pacific Financial Markets* **27**, 145 (2020).

[20] S. Kakinaka and K. Umeno, Cryptocurrency market efficiency in short- and long-term horizons during covid-19: An asymmetric multifractal analysis approach, *Finance Research Letters* **46**, 102319 (2022).

[21] T. Conlon and R. McGee, Safe haven or risky hazard? bitcoin during the covid-19 bear market, *Finance Research Letters* **35**, 101607 (2020).

[22] N. James, Dynamics, behaviours, and anomaly persistence in cryptocurrencies and equities surrounding COVID-19, *Physica A* **570**, 125831 (2021).

[23] N. James, M. Menzies, and J. Chan, Changes to the extreme and erratic behaviour of cryptocurrencies during COVID-19, *Physica A* **565**, 125581 (2021).

[24] Y.-J. Zhang, E. Bouri, R. Gupta, and S.-J. Ma, Risk spillover between bitcoin and conventional financial markets: An expectile-based approach, *The North American Journal of Economics and Finance* **55**, 101296 (2021).

[25] A. Elmelki, N. Chaâbane, and R. Benammar, Exploring the relationship between cryptocurrency and s&p500: evidence from wavelet coherence analysis, *International Journal of Blockchains and Cryptocurrencies* **3**, 256 (2022).

[26] M. Wątorek, J. Kwapień, and S. Drożdż, Cryptocurrencies are becoming part of the world global financial market, *Entropy* **25**, 377 (2023).

[27] J.-C. Li, Y.-Z. Xu, C. Tao, and G.-Y. Zhong, Multi-period impacts and network connectivity of cryptocurrencies to international stock markets, *Physica A* **658**, 130299 (2025).

[28] S. Choi and J. Shin, Bitcoin: an inflation hedge but not a safe haven, *Finance Research Letters* **46**, 102379 (2022).

[29] N. James, M. Menzies, and K. Chin, Economic state classification and portfolio optimisation with application to stagflationary environments, *Chaos, Solitons & Fractals* **164**, 112664 (2022).

[30] A. P. N. Nguyen, M. Crane, T. Conlon, and M. Bezbradica, Herding unmasked: Insights into cryptocurrencies, stocks and US ETFs, *PloS one* **20**, e0316332 (2025).

[31] K. Wu, S. Wheatley, and D. Sornette, Classification of cryptocurrency coins and tokens by the dynamics of their market capitalizations, *Royal Society open science* **5**, 180381 (2018).

[32] K. Duan, Y. Zhao, A. Urquhart, and Y. Huang, Do clean and dirty cryptocurrencies connect with financial assets differently? the role of economic policy uncertainty, *Energy Economics* **127**, 107079 (2023).

[33] A. P. N. Nguyen, T. T. Mai, M. Bezbradica, and M. Crane, Volatility and returns connectedness in cryptocurrency markets: Insights from graph-based methods, *Physica A* **632**, 129349 (2023).

[34] P. R. L. Alves, Time evolution of the chaos intensity of cryptocurrencies, *Nonlinear Dynamics* **113**, 5865 (2025).

[35] P. Bhattacharjee, S. Mishra, and S. H. Kang, Extreme frequency connectedness, determinants and portfolio analysis of major cryptocurrencies: Insights from quantile time-frequency approach, *The Quarterly Review of Economics and Finance* **100**, 101974 (2025).

[36] E. Bouri, S. Benbachir, and M. E. Alaoui, How Bitcoin market trends affect major cryptocurrencies?, *Physica A* **668**, 130587 (2025).

[37] F. Zhou and W. Guo, Multiscale spatiotemporal evolution analysis of cryptocurrency returns, *Applied Economics* , 1 (2025).

[38] D. Stosic, D. Stosic, T. B. Ludermir, and T. Stosic, Collective behavior of cryptocurrency price changes, *Physica A* **507**, 499 (2018).

[39] D. Zięba, R. Kokoszczyński, and K. Śledziewska, Shock transmission in the cryptocurrency market. is bitcoin the most influential?, *International Review of Financial Analysis* **64**, 102 (2019).

[40] A. Briola and T. Aste, Dependency structures in cryptocurrency market from high to low frequency, *Entropy* **24**, 1548 (2022).

[41] N. James and M. Menzies, Collective correlations, dynamics, and behavioural inconsistencies of the cryptocurrency market over time, *Nonlinear Dynamics* **107**, 4001 (2022).

[42] J. Y. Song, W. Chang, and J. W. Song, Cluster analysis on the structure of the cryptocurrency market via bitcoin–ethereum filtering, *Physica A* **527**, 121339 (2019).

[43] S. Drożdż, J. Kwapień, P. Oświęcimka, T. Stanisz, and M. Wątorek, Complexity in economic and social systems: Cryptocurrency market at around covid-19, *Entropy* **22**, 1043 (2020).

[44] J. Kwapień, M. Wątorek, and S. Drożdż, Cryptocurrency market consolidation in 2020–2021, *Entropy* **23**, 1674 (2021).

[45] N. James, Evolutionary correlation, regime switching, spectral dynamics and optimal trading strategies for cryptocurrencies and equities, *Physica D* **434**, 133262 (2022).

[46] R. Jing and L. E. Rocha, A network-based strategy of price correlations for optimal cryptocurrency portfolios, *Finance Research Letters* **58**, 104503 (2023).

[47] L. Jin, B. Zheng, X. Jiang, L. Xiong, J. Zhang, and J. Ma, Dynamic cross-correlation in emerging cryptocurrency market, *Physica A* **668**, 130568 (2025).

[48] R. N. Mantegna, Hierarchical structure in financial markets, *The European Physical Journal B* **11**, 193 (1999).

[49] J. P. Onnela, K. Kaski, and J. Kertész, Clustering and information in correlation based financial networks, *European Physical Journal B* **38**, 353 (2004).

[50] J. Kwapień, S. Gworek, S. Drożdż, and A. Górska, Analysis of a network structure of the foreign currency exchange market, *Journal of Economic Interaction and Coordination* **4**, 55 (2009).

[51] M. Tumminello, T. Aste, T. D. Matteo, and R. N. Mantegna, A tool for filtering information in complex systems, *PNAS*

102, 10421 (2005).

[52] M. Eryiğit and R. Eryiğit, Network structure of cross-correlations among the world market indices, *Physica A* **388**, 3551 (2009).

[53] M. Y. Hong and J. W. Yoon, The impact of covid-19 on cryptocurrency markets: A network analysis based on mutual information, *PLoS ONE* **17**, 10.1371/journal.pone.0259869 (2022).

[54] G. P. Massara, T. D. Matteo, and T. Aste, Network filtering for big data: Triangulated maximally filtered graph, *Journal of Complex Networks* **5**, 161 (2016).

[55] T. Millington, An investigation into the effects and effectiveness of correlation network filtration methods with financial returns, *PLoS ONE* **17**, 10.1371/journal.pone.0273830 (2022).

[56] V. Boginski, S. Butenko, and P. M. Pardalos, Statistical analysis of financial networks, *Computational Statistics and Data Analysis* **48**, 431 (2005).

[57] W. Q. Huang, X. T. Zhuang, and S. Yao, A network analysis of the chinese stock market, *Physica A* **388**, 2956 (2009).

[58] C. K. Tse, J. Liu, and F. C. Lau, A network perspective of the stock market, *Journal of Empirical Finance* **17**, 659 (2010).

[59] N. James, M. Menzies, and J. Chan, Semi-metric portfolio optimization: A new algorithm reducing simultaneous asset shocks, *Econometrics* **11**, 10.3390/econometrics11010008 (2023).

[60] N. James, M. Menzies, L. Azizi, and J. Chan, Novel semi-metrics for multivariate change point analysis and anomaly detection, *Physica D* **412**, 132636 (2020).

[61] J. Kwapień, P. Oświęcimka, and S. Drożdż, Detrended fluctuation analysis made flexible to detect range of cross-correlated fluctuations, *Physical Review E* **92**, 052815 (2015).

[62] J. Kwapień, P. Oświęcimka, M. Forczek, and S. Drożdż, Minimum spanning tree filtering of correlations for varying time scales and size of fluctuations, *Physical Review E* **95**, 052313 (2017).

[63] R. C. Prim, Shortest connection networks and some generalizations, *The Bell System Technical Journal* **36**, 1389 (1957).

[64] J. B. Kruskal, On the shortest spanning subtree of a graph and the traveling salesman problem, *Proceedings of the American Mathematical society* **7**, 48 (1956).

[65] N. Vandewalle, F. Brisbois, and X. Tordoir, Non-random topology of stock markets, *Quantitative Finance* **1**, 372 (2001).

[66] S. Maslov, Measures of globalization based on cross-correlations of world financial indices, *Physica A* **301**, 397 (2001).

[67] R. Coelho, S. Hutzler, P. Repetowicz, and P. Richmond, Sector analysis for a ftse portfolio of stocks, *Physica A* **373**, 615 (2007).

[68] M. A. Djauhari, A robust filter in stock networks analysis, *Physica A* **391**, 5049 (2012).

[69] J. Kwapień and S. Drożdż, Physical approach to complex systems, *Physics Reports* **515**, 115 (2012).

[70] D. Jun, S. Oh, and G. Kim, Analysis of the correlation network in the us stock market during january 2020, *Journal of the Korean Physical Society* **85**, 942 (2024).

[71] M. Wiliński, A. Sienkiewicz, T. Gubiec, R. Kutner, and Z. Struzik, Structural and topological phase transitions on the German Stock Exchange, *Physica A* **392**, 5963 (2013).

[72] J. Miśkiewicz and D. Bonarska-Kujawa, Evolving network analysis of S&P500 components: COVID-19 influence of cross-correlation network structure, *Entropy* **24**, 10.3390/e24010021 (2022).

[73] M. McDonald, O. Suleiman, S. Williams, S. Howison, and N. F. Johnson, Detecting a currency's dominance or dependence using foreign exchange network trees, *Physical Review E* **72**, 046106 (2005).

[74] A. Z. Górski, S. Drozdz, and J. Kwapień, Scale free effects in world currency exchange network, *European Physical Journal B* **66**, 91 (2008).

[75] G. J. Wang, C. Xie, F. Han, and B. Sun, Similarity measure and topology evolution of foreign exchange markets using dynamic time warping method: Evidence from minimal spanning tree, *Physica A* **391**, 4136 (2012).

[76] R. Gębarowski, P. Oświęcimka, M. Wątorek, and S. Drożdż, Detecting correlations and triangular arbitrage opportunities in the Forex by means of multifractal detrended cross-correlations analysis, *Nonlinear Dynamics* **98**, 2349 (2019).

[77] B. Li and Z. Liao, Finding changes in the foreign exchange market from the perspective of currency network, *Physica A* **545**, 123727 (2020).

[78] D. Zhang, Y. Zhuang, P. Tang, and Q. Han, The evolution of foreign exchange market: A network view, *Physica A* **608**, 128311 (2022).

[79] P. Sieczka and J. A. Holyst, Correlations in commodity markets, *Physica A* **388**, 1621 (2009).

[80] D. Matesanz, B. Torgler, G. Dabat, and G. J. Ortega, Co-movements in commodity prices: A note based on network analysis, *Agricultural Economics (United Kingdom)* **45**, 13 (2014).

[81] Y.-R. Ma, Q. Ji, F. Wu, and J. Pan, Financialization, idiosyncratic information and commodity co-movements, *Energy Economics* **94**, 105083 (2021).

[82] N. S. Magner, N. Hardy, J. Lavin, and T. Ferreira, Forecasting commodity market synchronization with commodity currencies: A network-based approach, *Entropy* **25**, 562 (2023).

[83] M. Durcheva and P. Tsankov, Analysis of similarities between stock and cryptocurrency series by using graphs and spanning trees, *AIP Conference Proceedings* **2172**, 090004 (2019).

[84] C. J. Francés, P. Grau-Carles, and D. J. Arellano, The cryptocurrency market: A network analysis, *Esic Market Economic and Business Journal* **49**, 569 (2018).

[85] K. Polovnikov, V. Kazakov, and S. Syntulsky, Core–periphery organization of the cryptocurrency market inferred by the modularity operator, *Physica A* **540**, 123075 (2020).

[86] N. Jaroonchokanan, A. Sinha, and S. Suwanna, Dynamics of network structure in cryptocurrency markets during abrupt changes in Bitcoin price, *Physica A* **661**, 130404 (2025).

[87] F. M. D. Collibus, C. Campajola, G. Caldarelli, and C. J. Tessone, Patterns and centralisation in ethereum-based token

transaction networks, *Frontiers in Physics* **12**, 1305167 (2024).

[88] M. Wątorek, P. Szydło, J. Kwapień, and S. Drożdż, Correlations versus noise in the NFT market, *Chaos* **34**, 073112 (2024).

[89] C.-K. Peng, S. V. Buldyrev, S. Havlin, M. Simons, H. E. Stanley, and A. L. Goldberger, Mosaic organization of dna nucleotides, *Physical Review E* **49**, 1685 (1994).

[90] J. W. Kantelhardt, S. A. Zschiegner, E. Koscielny-Bunde, S. Havlin, A. Bunde, and H. E. Stanley, Multifractal detrended fluctuation analysis of nonstationary time series, *Physica A* **316**, 87 (2002).

[91] B. Podobnik and H. E. Stanley, Detrended cross-correlation analysis: A new method for analyzing two nonstationary time series, *Physical Review Letters* **100**, 084102 (2008).

[92] W.-X. Zhou, Multifractal detrended cross-correlation analysis for two nonstationary signals, *Physical Review E* **77**, 066211 (2008).

[93] P. Oświęcimka, S. Drożdż, M. Forczek, S. Jadach, and J. Kwapień, Detrended cross-correlation analysis consistently extended to multifractality, *Physical Review E* **89**, 023305 (2014).

[94] G. J. Wang, C. Xie, Y. J. Chen, and S. Chen, Statistical properties of the foreign exchange network at different time scales: Evidence from detrended cross-correlation coefficient and minimum spanning tree, *Entropy* **15**, 1643 (2013).

[95] L. Zhao, W. Li, A. Fenu, B. Podobnik, Y. Wang, and H. E. Stanley, The q-dependent detrended cross-correlation analysis of stock market, *Journal of Statistical Mechanics: Theory and Experiment* **2018**, 023402 (2018).

[96] M. Lin, L. Zhao, and Y. Li, Nonlinear cross-correlation among worldwide indexes, *Journal of Physics: Conference Series* **1113**, 012017 (2018).

[97] P. Oświęcimka, J. Kwapień, and S. Drożdż, Wavelet versus detrended fluctuation analysis of multifractal structures, *Physical Review E* **74**, 016103 (2006).

[98] Z.-Q. Jiang, W.-J. Xie, W.-X. Zhou, and D. Sornette, Multifractal analysis of financial markets: a review, *Reports on Progress in Physics* **82**, 125901 (2019).

[99] G. Zebende, DCCA cross-correlation coefficient: Quantifying level of cross-correlation, *Physica A* **390**, 614 (2011).

[100] P. Embrechts, C. Klüppelberg, and T. Mikosch, *Modelling Extremal Events for Insurance and Finance*, Stochastic Modelling and Applied Probability (Springer, Berlin, Heidelberg, 1997).

[101] P. Gopikrishnan, M. Meyer, L. N. Amaral, and H. E. Stanley, Inverse cubic law for the distribution of stock price variations, *The European Physical Journal B* **3**, 139 (1998).

[102] Binance exchange, <https://www.binance.com/p1>.

[103] A dataset of 140 exchange rates from the Binance exchange, <https://doi.org/10.18150/WPGY4R>.

[104] CoinMarketCap, CoinMarketCap, <https://coinmarketcap.com>.

[105] CoinDesk DACSclassification, <https://indices.coindesk.com/indices/sector>.

[106] P. Oświęcimka, S. Drożdż, J. Kwapień, and A. Z. Górska, Effect of detrending on multifractal characteristics, *Acta Physica Polonica A* **123**, 597 (2013).

[107] A. Briola, D. Vidal-Tomás, Y. Wang, and T. Aste, Anatomy of a stablecoin's failure: The Terra-Luna case, *Finance Research Letters* **51**, 103358 (2023).

[108] D. Koutra, N. Shah, J. T. Vogelstein, B. Gallagher, and C. Faloutsos, Deltacon: Principled massive-graph similarity function with attribution, *ACM Transactions on Knowledge Discovery from Data (TKDD)* **10**, 1 (2016).

[109] N. D. Monnig and F. G. Meyer, The resistance perturbation distance: A metric for the analysis of dynamic networks, *Discrete Applied Mathematics* **236**, 347 (2018).

[110] V. Plerou, P. Gopikrishnan, B. Rosenow, L. A. Amaral, T. Guhr, and H. E. Stanley, Random matrix approach to cross correlations in financial data, *Physical Review E* **65**, 066126 (2002).

[111] R. Cont, Empirical properties of asset returns: stylized facts and statistical issues, *Quantitative Finance* **1**, 223 (2001).

[112] M. Ausloos, Statistical physics in foreign exchange currency and stock markets, *Physica A* **285**, 48 (2000).

[113] R. Kutner and F. Świtła, Remarks on the possible universal mechanism of the non-linear long-term autocorrelations in financial time-series, *Physica A* **344**, 244 (2004).

[114] S. Drożdż, J. Kwapień, and M. Wątorek, What is mature and what is still emerging in the cryptocurrency market?, *Entropy* **25**, 10.1080/713665670 (2023).